Pulsed-Field Gradient Nuclear Magnetic Resonance as a Tool for Studying Translational Diffusion: Part 1. Basic Theory

WILLIAM S. PRICE

Water Research Institute, Sengen 2-1-6, Tsukuba, Ibaraki 305, Japan

ABSTRACT: Translational diffusion is the most fundamental form of transport in chemical and biochemical systems. Pulsed-field gradient nuclear magnetic resonance provides a convenient and noninvasive means for measuring translational motion. In this method the attenuation of the echo signal from a Hahn spin-echo pulse sequence containing a magnetic field gradient pulse in each τ period is used to measure the displacement of the observed spins. In the present article, the physical basis of this method is considered in detail. Starting from the Bloch equations containing diffusion terms, the (analytical) equation linking the echo attenuation to the diffusion of the spin for the case of unrestricted isotropic diffusion is derived. When the motion of the spin occurs within a confined geometry or is anisotropic, such as in *in vivo* systems, the echo attenuation also yields information on the surrounding structure, but as the analytical approach becomes mathematically intractable, approximate or numerical means must be used to extract the motional information. In this work, two common approximations are considered and their limitations are examined. Measurements in anisotropic systems are also considered in some detail.
© 1997 John Wiley & Sons, Inc. Concepts Magn Reson **9:** 299–336, 1997

KEY WORDS: diffraction, diffusion, molecular dynamics, pulse field gradient, restricted diffusion

---

Received July 18, 1996; revised May 5, 1997; accepted May 9, 1997.

Address for correspondence: Dr. William S. Price, Water Research Institute, Sengen 2-1-6, Tsukuba, Ibaraki 305, Japan. Ph: (81-298) 58 6186, FAX: (81-298) 58 6144. e-mail: wprice@wri.co.jp.

© 1997 John Wiley & Sons, Inc. CCC 1043-7347/97/050299-37

INTRODUCTION

Self-diffusion is the random translational motion of molecules (or ions) driven by internal kinetic energy. Translational diffusion (not to be confused with spin diffusion or rotational diffusion) is the most fundamental form of transport (*1–3*) and is responsible for all chemical reactions, since the reacting species must collide before they can react (*4*). Diffusion is also closely related to molecular size, as can be seen from the Stokes–Einstein equation,

$$D = \frac{kT}{f} \qquad [1]$$

where k is the Boltzmann constant, T is temperature, and f is the friction coefficient. For the simple case of a spherical particle with an effective hydrodynamic radius (i.e., Stokes radius) r_S in a solution of viscosity η the friction factor is given by

$$f = 6\pi\eta r_S. \qquad [2]$$

Generally, however, molecular shapes are more complicated and may include contributions from factors such as hydration, and the friction factor must be modified accordingly (*4–9*). As a consequence, the diffusion also provides information on the interactions and shape of the diffusing molecule.

Because of its noninvasive nature, nuclear magnetic resonance (NMR) spectroscopy is a unique tool for studying molecular dynamics in chemical and biological systems (*10–19*). There are two main ways in which NMR may be used to study self-diffusion coefficients, which are also known as tracer-diffusion or intradiffusion coefficients (*11, 13, 20*) (Fig. 1): (a) analysis of relaxation data [e.g., Refs. (*21, 22*)] and (b) pulsed-field gradient (PFG) NMR. However, the two methods report on motions in very different time scales and thus, even though a translational diffusion coefficient can be derived in both cases, the two estimates will agree only under certain circumstances (*23*) since the relaxation method is in fact sensitive to rotational diffusion, whereas the PFG method measures translational diffusion. Generally, in experiments involving the solution state, relaxation measurements are sensitive to motions occurring in the picosecond to nanosecond time scale—that is, motion on the time scale of the reorientational correlation of the nucleus. While in PFG measurements, motion is measured over the millisecond to second time scale.

In the first method, relaxation data are analyzed to determine the rotational correlation time(s) (τ_c) of a probe species (*24*). τ_c can then be related to the solution viscosity, and ultimately, to the translational diffusion coefficient (Fig. 1) by using the Debye equation (*25–27*),

$$\tau_c = 4\pi\eta r_S^3/(3kT) \qquad [3]$$

and the Stokes–Einstein equation (i.e., Eq. [1]). However, a number of assumptions which, depending upon the system being studied, may or may not be justified need to be made in performing this analysis. First, the relaxation mechanism of the probe species needs to be known, and it is required that the intermolecular contributions to the relaxation can be separated from the intramolecular contributions (*28*). Second, only if the molecule is spherical can its rotational dynamics be properly characterized by a single correlation time. Third, depending on the size of the probe molecules compared to the molecules of the bulk solution, they may not see the solution as being continuous; as a consequence, one of the basic requirements for the validity of the Debye equation is violated (*8, 9*). Thus, serious assumptions are involved in applying this method to studying biological systems when a small probe species is used since the solution normally has a large macromolecular component (e.g., a large part of the cytoplasm of red blood cells is composed of hemoglobin). The final problem with this method is that the Stokes radius of the probe molecule needs to be known and the determination of this is not straightforward.

In the PFG method, the attenuation of a spin-echo signal resulting from the dephasing of the nuclear spins due to the combination of the translational motion of the spins and the imposition of spatially well-defined gradient pulses is used to measure motion. In contradistinction to the relaxation method, no assumptions need to be made regarding the relaxation mechanism(s) or in relating τ_c to the translational motion of the probe molecule. However, to determine the "true" diffusion coefficient, D, as against an "apparent" diffusion coefficient D_{app} the effects of structural boundaries that affect the natural diffusion of the probe species need to be considered. The mathematics required to model anything except for free diffusion or diffusion within simple geometries becomes rather complicated, and as a result, ana-

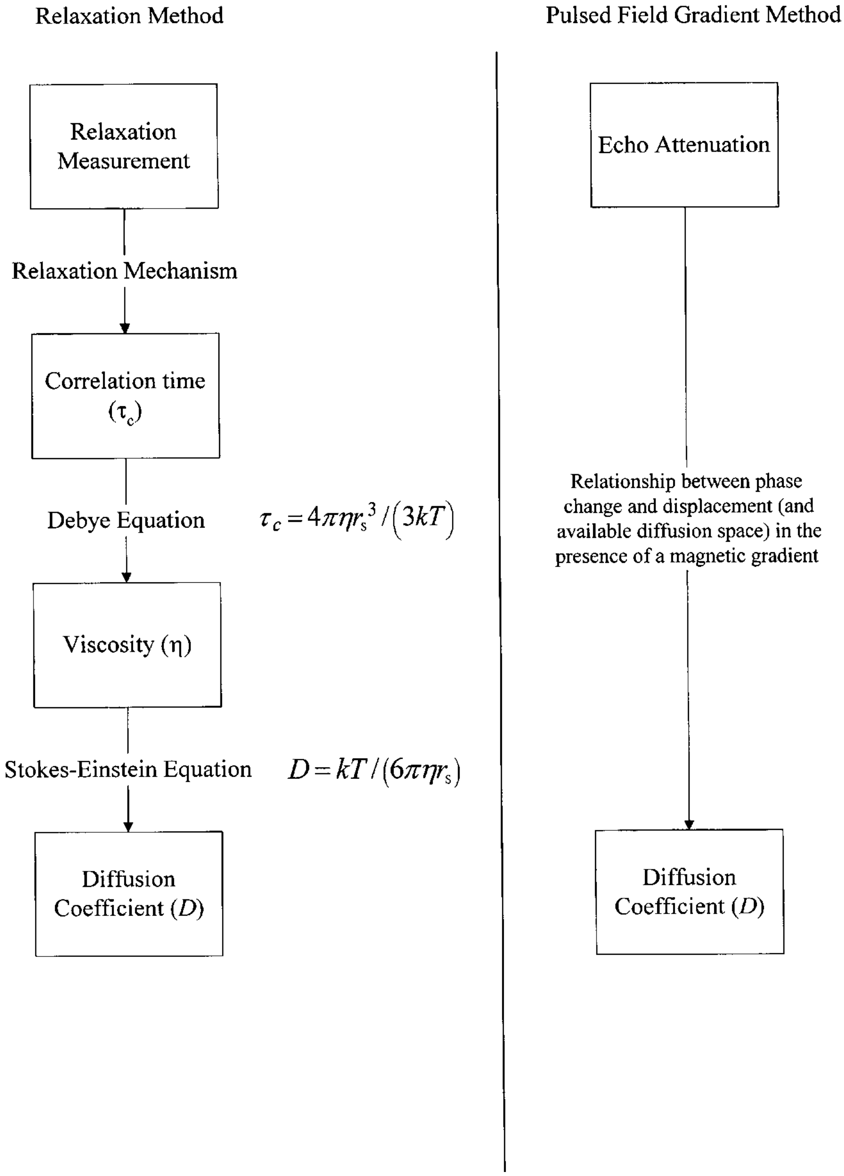
Relaxation Method
Pulsed Field Gradient Method
Relaxation Measurement
Relaxation Mechanism
Correlation time (τ_c)
Debye Equation
$\tau_c = 4\pi\eta r_s^3/(3kT)$
Viscosity (η)
Stokes-Einstein Equation
$D = kT/(6\pi\eta r_s)$
Diffusion Coefficient (D)
Echo Attenuation
Relationship between phase change and displacement (and available diffusion space) in the presence of a magnetic gradient
Diffusion Coefficient (D)

Figure 1 Schematic representation of the relaxation and pulsed-field gradient methods for determining molecular dynamics. In our representation of the relaxation method, we have assumed that the probe molecule is a sphere with an effective hydrodynamic radius of r_S.

lytical solutions are generally not possible and numerical solutions must be sought.

In practice, both B_0 (i.e., magnetic) and B_1 [i.e., radiofrequency (rf)] gradients (*15, 29, 30*) can be used, but in the present article we will concentrate on B_0 gradients, although it should be noted that the theoretical aspects are generally analogous. The application of B_0 gradients to high-resolution NMR is now commonplace and provides superior methods of water suppression, coherence selection, and quadrature detection, and methods for controlling the effects of radiation damping (*15, 19, 31–40*). Gradients also provide the basis of spatial resolution in NMR microscopy and imaging [i.e., magnetic resonance imaging (MRI)] (*41–44*), but the application of B_0 gradients to the study of molecular dynamics is less widespread. Gradients afford a powerful tool not only for studying molecular diffusion (under favorable circumstances down to $< 10^{-17}\ \mathrm{m^2 s^{-1}}$), but also for providing structural information in the range of 0.1–100 μm when the diffusion is restricted (e.g., diffusion in a cell) on the NMR time scale. The use of magnetic field gradients allows diffusion to be added to the standard NMR observables of chemical shifts and relaxation times (i.e., longitudinal or T_1; transverse or T_2; and in the rotating frame or $T_{1\rho}$). Gradient-based diffusion measurements have been found to have clinical utility in NMR imaging studies (*45–49*) especially in regard to study of cerebral ischaemia [e.g., Ref. (*50*) and references therein].

The aim of this article is to present an introduction to the PFG experiment and the theoretical basis used for interpreting the data, to determine the diffusion coefficient of a probe species and perhaps information on the geometry in which it is diffusing. As it is not possible to provide a comprehensive review of the literature in a single paper, a number of pertinent references have been mentioned in the text that may be consulted for more in-depth coverage of some aspects. The analysis of PFG NMR experiments is inherently mathematical, and general books on mathematical methods [e.g., Ref. (*51*)], mathematical functions [e.g., Ref. (*52*)], and integrals [e.g., Ref. (*53*)] are useful references. Particular emphasis is placed on developing a physical feeling for the PFG method. It should be noted that the theory presented is quite general and applies equally to both *in vivo* and *in vitro* samples. In the next section, the effects of a magnetic gradient on nuclear spins is discussed, followed by an intuitive explanation of how diffusion can be related to the attenuation of the echo signal in the PFG NMR experiment. Finally, the concept of restricted diffusion is introduced. In the third section, the mathematical background relating diffusion to the echo attenuation and the experimental parameters is considered in detail. First, an analytical macroscopic approach starting from the Bloch equation is derived. The effects of flow superimposed upon diffusion are also considered. Next, two common approximate methods, the Gaussian phase distribution (GPD) approximation and the short gradient pulse (SGP) approximation, are presented. To illustrate these approaches, equations relating echo attenuation to the experimental variables and the diffusion coefficient are derived for the case of free diffusion. The analogy between PFG measurements and scattering is explained. Finally, the concepts of "diffusive diffraction" and of imaging molecular motion are illustrated using diffusion within a rectangular barrier pore as an example. In the final section, we consider the general relationships between the experimental variables and echo attenuation in restricted geometries and the validity of the GPD and SGP approximations. The differences and similarities between the two approaches are elucidated pictorially using the example of diffusion in a sphere. PFG diffusion measurements in anisotropic systems, which commonly occur in liquid crystal and *in vivo* studies, are examined in the last subsection of the article.

NUCLEAR SPINS, GRADIENTS, AND DIFFUSION

Magnetic Gradients as Spatial Labels

All of the NMR theory needed for understanding the effects of B_0 gradients on nuclear spins has the Larmor equation as the origin:

$$\omega_0 = \gamma B_0 \qquad [4]$$

where ω_0 is the Larmor frequency (radians s^{-1}), γ is the gyromagnetic ratio (rad T^{-1} s^{-1}), B_0(T) is the strength of the static magnetic field, and we have neglected the small effect of the shielding constant. We consider $\mathbf{B}_0$ to be oriented in the z-direction. Since B_0 is spatially homogeneous, ω is the same throughout the sample. Equation [4] holds for a single quantum coherence (i.e., $n = 1$). However, if in addition to $\mathbf{B}_0$ there is a spatially dependent magnetic field gradient $\mathbf{g}$ (T m^{-1}), and accounting for the possibility of more than single quantum coherence, ω becomes spatially dependent,

$$\omega_{eff}(n, \mathbf{r}) = n(\omega_0 + \gamma(\mathbf{g} \cdot \mathbf{r})) \qquad [5]$$

where we define $\mathbf{g}$ by the **grad** of the gradient field component parallel to $\mathbf{B}_0$, i.e.,

$$\mathbf{g} = \nabla \mathbf{B}_0 = \frac{\partial \mathbf{B}_z}{\partial x}\mathbf{i} + \frac{\partial \mathbf{B}_z}{\partial y}\mathbf{j} + \frac{\partial \mathbf{B}_z}{\partial z}\mathbf{k} \qquad [6]$$

where $\mathbf{i}$, $\mathbf{j}$, and $\mathbf{k}$ are unit vectors of the laboratory frame of reference. The important point is that if a homogeneous gradient of known magnitude is imposed throughout the sample, the Larmor frequency becomes a spatial label with respect to the direction of the gradient. In imaging systems, which typically can produce equally strong magnetic field gradients in each of the x, y, and z directions, it is possible to measure diffusion along any of the x, y, or z-directions (or combinations thereof); however, in normal NMR spectrometers, it is more common to measure diffusion with the gradient oriented along the z-axis (i.e., parallel to $\mathbf{B}_0$). For simplicity, in most of the present article we are concerned only with the case where the gradient is oriented along z, although some attention is paid to the use of gradients along more than one axis when we consider anisotropic diffusion in the final subsection. In the case of a single gradient oriented along z, the magnitude of $\mathbf{g}$ is only a function of the position on the z-axis, $g_z = \mathbf{g} \cdot \mathbf{k}$, which we will henceforth refer to simply as g. It can be seen from Eq. [5] that successively higher (homonuclear) quantum transitions are more sensitive to the effects of the gradient, whereas zero quantum transitions are unaffected by the presence of the gradient. For heteronuclear multiple quantum transitions, Eq. [5] must be modified to account for the coherent spins.

In the case of a single quantum coherence, we can see from Eq. [5] that for a single spin the cumulative phase shift is given by

$$\phi(t) = \underbrace{\gamma B_0 t}_{\text{static field}} + \underbrace{\gamma \int_0^t g(t') z(t')\, dt'}_{\text{applied gradient}} \qquad [7]$$

where the first term on the right-hand side corresponds to the phase shift due to the static field, and the second term represents the phase shift due to the effects of the gradient. Thus, from the second term of Eq. [7] we can see that the degree of dephasing due to the gradient pulse is proportional to the type of nucleus (i.e., γ), the strength of the gradient (i.e., g), the duration of the gradient (i.e., t), and the displacement of the spin along the direction of the gradient. Although the gradient is normally applied in a pulse of constant amplitude, we have written g as $g(t)$ in Eq. [7] to emphasize that the gradient may itself be a function of time (i.e., not merely a rectangular pulse). However, for simplicity, in the present article we will concern ourselves only with constant amplitude pulses. In this case we can think of the "area" or "dephasing strength" of the gradient pulse as equaling $\gamma g t$.

Measuring Diffusion with Magnetic Field Gradients

From Eq. [5] it is apparent that a (well-defined) magnetic field gradient can be used to label the position of a spin, albeit indirectly, through the Larmor frequency. This provides the basis for measuring diffusion. The most common approach is to use a simple modification (*54–56*) of the Hahn spin-echo pulse sequence (*57–59*), in which equal rectangular gradient pulses of duration δ are inserted into each τ period (the "Stejskal and Tanner sequence" or "PFG sequence") (Fig. 2). Applying the magnetic field gradient in pulses instead of continuously [i.e., steady gradient experiment (*57, 58*)] circumvents a number of experimental limitations (*54*): (a) Since the gradient is off during acquisition, the line width is not broadened by the gradient, and thus the method is suitable for measuring the diffusion coefficient of more than one species simultaneously. (b) The rf power does not have to be increased to cope with a gradient-broadened spectrum. (c) Smaller diffusion coefficients can be measured since it is possible to use larger gradients. (d) The time over which diffusion is measured is well defined because the gradient is applied in pulses; this is of particular importance to studies of restricted diffusion (see the next section). (e) As the gradient is applied in pulses it is (normally) possible to separate the effects of diffusion from spin–spin relaxation; this will be explained below. Generally, the applied gradient pulses are much stronger than any background gradients that may be present; as a result, the background gradients (e.g., due to differences in susceptibility in the sample, inhomogeneities in the main magnetic field, etc.) will be neglected in the analysis given below.

We will now qualitatively explain how this method works. The mechanism is shown schematically in Fig. 2. Imagine that we have an ensemble of diffusing spins at thermal equilibrium (i.e., the net magnetization is oriented along the z-axis). A $\pi/2$ rf pulse is applied which rotates the macroscopic magnetization from the z-axis into the x–y plane (i.e., perpendicular to the static field). During the first τ period at time t_1, a gradient pulse of duration δ and magnitude g is applied so that at the end of the first τ period, spin i experiences a phase shift,

$$\phi_i(\tau) = \underbrace{\gamma B_0 \tau}_{\text{static field}} + \underbrace{\gamma g \int_{t_1}^{t_1+\delta} z_i(t)\, dt}_{\text{applied gradient}} \qquad [8]$$

where the first term is the phase shift due to the main field, and the second one due to the gradient. Different from Eq. [7] we have taken g out of the integral in Eq. [8] since we are considering a constant amplitude gradient.

At the end of the first τ period, a π rf pulse is applied that has the effect of reversing the sign of the precession (i.e., the sign of the phase angle) or, equivalently, the sign of the applied gradients and static field. At time $t_1 + \Delta$, a second gradient pulse of equal magnitude and duration is applied (n.b., the π pulse has the effect of changing the sign of the first gradient pulse; this leads to the idea of an "effective" field gradient; see The Macroscopic Approach). If the spins have not undergone any translational motion with respect to the z-axis, the effects of the two applied gradi-

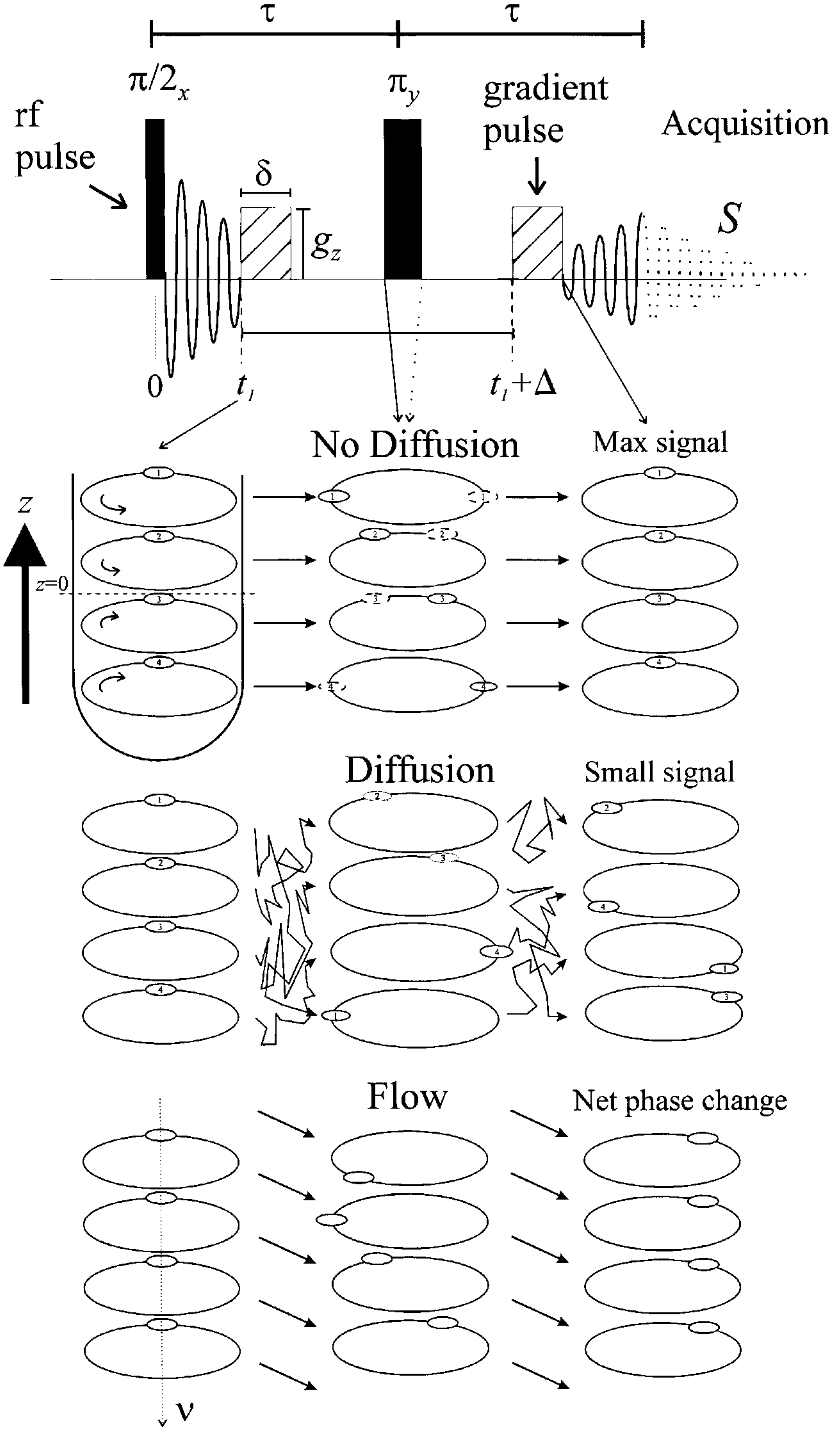
τ
τ
π/2x
πy
rf pulse
gradient pulse
Acquisition
δ
gz
S
0
t1
t1+Δ
No Diffusion
Max signal
z
z=0
1
2
3
4
Diffusion
Small signal
Flow
Net phase change
v

ent pulses cancel and all spins refocus. However, if the spins have moved, the degree of dephasing due to the applied gradient is proportional to the displacement in the direction of the gradient (i.e., the z-direction) in the period Δ (i.e., the duration between the leading edges of the gradient pulses). Thus, at the end of the echo sequence, the total phase shift of spin i relative to being located at $z = 0$ is given by

$$\begin{aligned}\phi_i(2\tau) &= \underbrace{\left\{\gamma B_0\tau + \gamma g\int_{t_1}^{t_1+\delta} z_i(t)\,dt\right\}}_{\text{first } \tau \text{ period}} \\ &\quad - \underbrace{\left\{\gamma B_0\tau + \gamma g\int_{t_1+\Delta}^{t_1+\Delta+\delta} z_i(t')\,dt'\right\}}_{\text{second } \tau \text{ period}} \\ &= \gamma g\left\{\int_{t_1}^{t_1+\delta} z_i(t)\,dt - \int_{t_1+\Delta}^{t_1+\Delta+\delta} z_i(t')\,dt'\right\}\end{aligned} \qquad [9]$$

We should recall that in NMR we are concerned with an ensemble of nuclei (with different spatial starting and finishing positions), and thus, the normalized intensity (i.e., an attenuation) of the echo signal at $t = 2\tau$ [i.e., $S(2\tau)$] is given by (*58, 60*),

$$S(2\tau) = S(2\tau)_{g=0}\int_{-\infty}^{\infty} P(\phi, 2\tau)e^{i\phi}\,d\phi. \qquad [10]$$

where $S(2\tau)_{g=0}$ is the signal (i.e., resultant magnetic moment) in the absence of a field gradient. If we consider only the real component of $S(2\tau)$, and recalling De Moivre's theorem,

$$e^{i\phi} = \cos\phi + i\sin\phi \qquad [11]$$

we have

$$S(2\tau) = S(2\tau)_{g=0}\int_{-\infty}^{\infty} P(\phi, 2\tau)\cos\phi\,d\phi \qquad [12]$$

where $P(\phi, 2\tau)$ is the (relative) phase-distribution function. For the PFG sequence, some authors write $P(\phi, \Delta)$, since it is the gradient pulses and the separation between them that constitute the

Figure 2 A schematic representation of how the Stejskal and Tanner (or PFG) pulse sequence measures diffusion and flow. This is a Hahn spin-echo pulse sequence with a rectangular gradient pulse of duration δ and magnitude g inserted into each τ delay. The separation between the leading edges of the gradient pulses is denoted by Δ. The applied gradient is generally along the z-axis (the direction of the static field). The second half of the echo is digitized (denoted by dots) and used as the free induction decay (FID). In this schematic description, we assume that we start the pulse sequence with a sample consisting of four in-phase spins (really an ensemble!) and we consider only the precession due to the gradient (i.e., we use a rotating reference frame rotating at ω_0). We assume that the center of the gradient coincides with the center of the sample (i.e., $z = 0$). Accordingly, the spins above and below this point acquire phase shifts owing to the gradient pulses, but in opposite senses. In the absence of diffusion, the effect of the first gradient pulse, denoted by the curved arrows in the first phase diagram, is to create a magnetization helix (i.e., the solid ellipses in the center phase diagram) with a pitch of $2\pi/(\gamma\delta g)$. Although we have represented the gradient pulses as having a finite width it is easier to consider them in the limit of $\delta \rightarrow 0$ (i.e., the short gradient pulse limit). The π pulse reverses the sign of the phase angle (i.e., the dotted ellipses in the center phase diagram), and thus, after the second gradient pulse, the helix is unwound and all spins are in phase, which gives a maximum echo signal. In the presence of diffusion, the winding and unwinding of the helix are scrambled by the diffusion process, resulting in a distribution of phases, although it is not easily seen since our sample consists of only four spins. Larger diffusion would be reflected by poorer refocusing of the spins, and consequently by a smaller echo signal. The effects of restriction upon the diffusion process will also contribute to this loss of phase coherence. In the absence of any background gradients, diffusion in the periods before (e.g., $0 \rightarrow t_1$) and after (i.e., $t_1 + \Delta + \delta$) the gradient pulses does not affect the signal attenuation. In the presence of flow (imagine that the outflowing spins are replaced by inflowing spins) along the direction of the gradient (in the $-z$ direction with velocity v in the present example) and neglecting diffusion, all the spins receive the same change in phase. The greater the flow is, the larger is the net phase change. If both diffusion and flow processes are present, then the whole diffusion-induced phase distribution receives a net phase shift.

"active" part of the sequence. By definition, $P(\phi, 2\tau)$ must be a normalized function, and so

$$\int_{-\infty}^{\infty} P(\phi, 2\tau)\, d\phi = 1. \qquad [13]$$

Below, we will consider the further derivation of Eq. [12] in the context of the GPD approximation (see The GPD Approximation). However, for the present, Eqs. [9] and [12] provide a very clear conceptual idea as to how the PFG method works. From Eq. [9], it can be seen that the phase shift due to the static field cancels. In the absence of diffusion, the phase shifts due to the two gradient pulses (or, conversely, in the presence of diffusion but with $g = 0$) will also cancel; thus, $\phi_i = 0$ for all i, and as $\cos\phi = 1$ in Eq. [12], a maximum signal will be recorded (see the first series of phase diagrams in Fig. 2). However, if we have diffusion, then the displacement function $z_i(t)$ is time dependent and the phase shifts accumulated by an individual nucleus due to the action of the gradient pulses in the first and second τ periods (during the gradient pulses to be precise see Eq. [9]; n.b., we neglect the effects of background gradients) do not cancel. The degree of miscancellation (i.e., larger phase shift) increases with increasing displacement due to diffusion (i.e., random motion) along the gradient axis. These random phase shifts resulting from the diffusion are averaged over the whole ensemble of nuclei that contribute to the NMR signal. Hence, the observed NMR signal is not phase shifted but attenuated, and the greater the diffusion is, the larger is the attenuation of the echo signal (see the second series of phase diagrams in Fig. 2). Similarly, as the gradient strength is increased in the presence of diffusion the echo signal attenuates. In Fig. 3 some experimental ^{13}C-NMR PFG spectra of $^{13}CCl_4$ are presented to illustrate the loss of echo signal intensity due to diffusion. Net flow, on the other hand, causes a net phase shift of the echo signal (see the third series of phase diagrams in Fig. 2 and the end of this subsection) instead of the diffusion-induced "blurring" of the phases which results in a diminution of the echo signal.

It is important to understand the difference between gradient echoes and spin echoes. In measuring diffusion, we generally choose to use the PFG pulse sequence (i.e., a spin-echo sequence) instead of a gradient-echo pulse sequence (i.e., the PFG pulse sequence without the π pulse and with the second gradient pulse having an opposite polarity to the first pulse). The reason is that as well as refocusing the sign of the phase angle accumulated during the first τ period, the π pulse has the effect of refocusing chemical shifts and the frequency dispersion due to the residual B_0 inhomogeneity and susceptibility effects in heterogeneous samples, etc. A gradi-

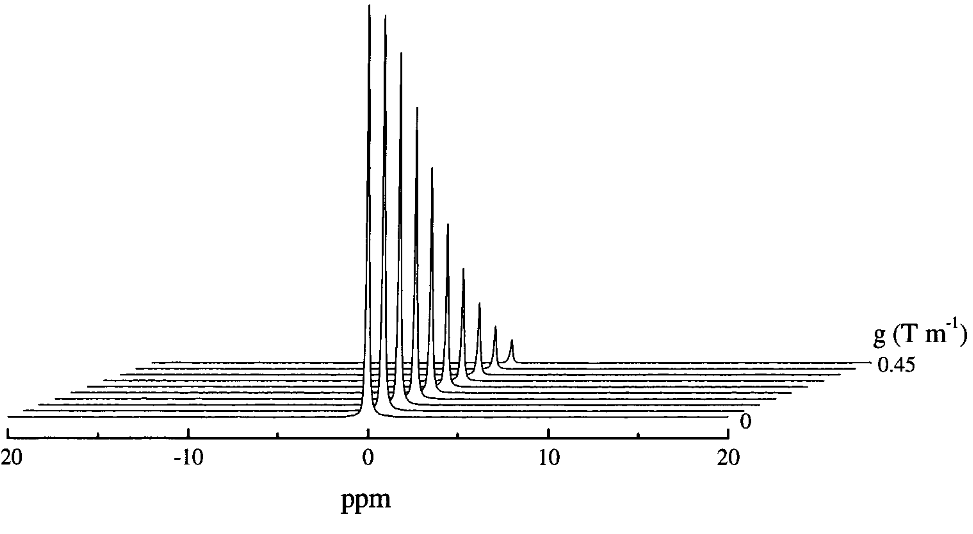

Figure 3 ^{13}C-PFG NMR spectra of a sample of $^{13}CCl_4$. The spectra were acquired at 303 K with $\Delta = 100$ ms, $\delta = 4$ ms, and g ranging from 0 to 0.45 T m^{-1} in 0.05-T m^{-1} increments. The spectra are presented in phase-sensitive mode with a line broadening of 5 Hz. As the intensity of the gradient increases, the echo intensity decreases due to the effects of diffusion.

ent echo, on the other hand, refocuses only the phase dispersion resulting from the gradient pulses. It is because of the additional properties of spin echoes that diffusion measurements are almost invariably performed using spin-echo–based sequences.

In our discussion above, we did not consider the relaxation process that occurs during the echo sequence. Thus, in the absence of diffusion and/or the absence of gradients, we would have the signal at $t = 2\tau$ equal to

$$S(2\tau)_{g=0} = S(0)\exp\left(-\frac{2\tau}{T_2}\right) \qquad [14]$$

where $S(0)$ is the signal without attenuation due to relaxation–that is, the signal that would be observed immediately after the $\pi/2$ pulse. We assume here that the observed signal originates from a single species (i.e., the observed signal results from one population with a single relaxation time). In the presence of diffusion and gradient pulses, the attenuation due to relaxation and the attenuation due to diffusion and the applied gradient pulses are independent, and so we can write,

$$S(2\tau) = S(0)\ \underbrace{\exp\left(-\frac{2\tau}{T_2}\right)}_{\text{attenuation due to relaxation}}\ \underbrace{f(\delta, g, \Delta, D)}_{\text{attenuation due to diffusion}} \qquad [15]$$

where $f(\delta, g, \Delta, D)$ is a function that represents the attenuation due to diffusion (e.g., compare Eq. [15] with Eq. [10]). Thus, if the PFG measurement is performed whilst keeping τ constant, it is possible to separate the contributions. Hence, by dividing Eq. [15] by Eq. [14] we normalize out the attenuation due to relaxation, leaving only the attenuation due to diffusion,

$$E = \frac{S(2\tau)}{S(2\tau)_{g=0}} = f(\delta, g, \Delta, D). \qquad [16]$$

In the steady-gradient experiment (i.e, $\Delta = \delta = \tau$), however, since the gradients are on for all of the sequence, only g can be altered independently of τ. Recall the well-known diffusion term in the expression for the intensity of the Hahn spin-echo sequence (*57–59*),

$$S(2\tau) = S(0)\underbrace{\exp(-2\tau/T_2)}_{\text{attenuation due to relaxation}}\ \underbrace{\exp(-2\gamma^2 D g^2 \tau^3/3)}_{\text{attenuation due to diffusion}}, \qquad [17]$$

whereas in the PFG experiment, we can alter δ, Δ, or g independently of τ and still perform this normalization. This is a very important distinction between the steady-gradient diffusion experiment and the PFG experiment.

Although the effects of relaxation are normalized out, since we use E as our experimental measure, the time scale of the experiment (i.e, Δ) is limited by the relaxation time of the probe species. As Δ increases, so must τ, and eventually the signal will become too small to measure (see Eq. [14]). The smallest value of Δ will be limited by the performance of the gradient system. In practice, Δ is normally between 1 ms and 1 s. δ must be smaller than Δ and is typically in the range of 0–10 ms. The magnitude of g is machine dependent, and currently the largest gradient pulses on commercially available equipment are of the order of 20 T m^{-1}.

We now need to equate the attenuation (E) of the echo signal to the experimental variables; that is, we need to derive $f(\delta, g, \Delta, D)$. The methods for doing this will be presented in the next section. However, we first need to digress a little and consider diffusion itself.

Free and Restricted Diffusion

In the PFG experiment, we probe the particle's motion by taking a measurement at time $t = t_1$ and a second measurement at time $t = t_1 + \Delta$. The key point is that in the PFG experiment the echo attenuation gives information on the displacement along the gradient axis (the z-axis in the present case) that has occurred during the period Δ, which can then be related to the diffusion coefficient but it does not, at least directly, give us information on how the particle moved between the initial and the final positions. Specifically, it gives information on the self-correlation function (61), $P(\mathbf{r}_0, \mathbf{r}_1, t)$—that is, the conditional probability of finding a particle initially at a position $\mathbf{r}_0$, at a position $\mathbf{r}_1$ after a time t. $P(\mathbf{r}_0, \mathbf{r}_1, t)$ is given by the solution of the diffusion equation. Hence we need to examine the diffusion equation and how we can obtain $P(\mathbf{r}_0, \mathbf{r}_1, t)$ from it.

In terms of the concentration in number of particles per unit volume, $c(\mathbf{r},t)$, the flux of a particle is given by Fick's first law of diffusion to be [for example, see Ref. (*2, 62*)],

$$\mathbf{J}(\mathbf{r},t) = -D\nabla c(\mathbf{r},t). \qquad [18]$$

The minus sign indicates that (in isotropic media) the direction of flow is from larger to smaller concentration. Because of the conservation of mass, the continuity theorem applies, and thus,

$$\frac{\partial c(\mathbf{r},t)}{\partial t} = -\nabla \cdot \mathbf{J}(\mathbf{r},t). \qquad [19]$$

In other words, Eq. [19] states that $\partial c(\mathbf{r},t)/\partial t$ is the difference between the influx and efflux from the point located at $\mathbf{r}$. Combining Eqs. [18] and [19] we arrive at Fick's second law of diffusion [e.g., Refs. (*4, 51, 62*)],

$$\frac{\partial c(\mathbf{r},t)}{\partial t} = D\nabla^2 c(\mathbf{r},t) \qquad [20]$$

So far in our mathematical descriptions of diffusion, we have, perhaps simplistically, assumed that the diffusion process is isotropic and can therefore be described by the isotropic diffusion coefficient D (i.e., a scalar). More generally the diffusion process is represented by a cartesian, or rank two, tensor (i.e., a 3×3 matrix) (*51*), $\mathbf{D}$ ($D_{\alpha\beta}$ where α and β take each of the Cartesian directions); thus, written more generally, Eq. [18] can be written as

$$\mathbf{J}(\mathbf{r},t) = -\mathbf{D}\nabla c(\mathbf{r},t), \qquad [21]$$

which is shorthand for

$$\begin{bmatrix} J(x,t) \\ J(y,t) \\ J(z,t) \end{bmatrix} = -\begin{bmatrix} D_{xx} & D_{xy} & D_{xz} \\ D_{yx} & D_{yy} & D_{yz} \\ D_{zx} & D_{zy} & D_{zz} \end{bmatrix} \begin{bmatrix} \dfrac{\partial c(x,t)}{\partial x} \\ \dfrac{\partial c(y,t)}{\partial y} \\ \dfrac{\partial c(z,t)}{\partial z} \end{bmatrix}. \qquad [22]$$

We note that the diagonal elements of $\mathbf{D}$, (e.g., $\alpha = \beta$) scale concentration gradients and fluxes in the same direction, the off-diagonal elements (e.g., $\alpha \neq \beta$) couple fluxes and concentration gradients in orthogonal directions, and similarly, Eq. [20] becomes

$$\frac{\partial c(\mathbf{r},t)}{\partial t} = \nabla \cdot \mathbf{D}\nabla c(\mathbf{r},t). \qquad [23]$$

For simplicity in most of what follows, we are concerned only with isotropic diffusion. However, in the section on anisotropic diffusion, we will consider in detail the significance of anisotropic diffusion in PFG diffusion measurements.

In the case of self-diffusion, there is no net concentration gradient, and instead we are concerned with the total probability, $P(\mathbf{r}_1,t)$ of finding a particle at position $\mathbf{r}_1$ at time t. This is given by

$$P(\mathbf{r}_1,t) = \int \rho(\mathbf{r}_0) P(\mathbf{r}_0,\mathbf{r}_1,t)\, d\mathbf{r}_0 \qquad [24]$$

where $\rho(\mathbf{r}_0)$ is the particle density (the formal definition of the particle density is considered in detail below), and thus, $\rho(\mathbf{r}_0)P(\mathbf{r}_0,\mathbf{r}_1,t)$ is the probability of starting from $\mathbf{r}_0$ and moving to $\mathbf{r}_1$ in time t. The integration over $\mathbf{r}_0$ accounts for all possible starting positions. Similar to concentration, $P(\mathbf{r}_1,t)$ describes the probability of finding a particle in a certain place at a certain time. $P(\mathbf{r}_1,t)$ is a sort of ensemble-averaged probability concentration for a single particle, and it is thus reasonable to assume that it obeys the diffusion equation (*41*). Because the spatial derivatives in Fick's laws refer to $\mathbf{r}_1$, we can rewrite Fick's laws in terms of $P(\mathbf{r}_0,\mathbf{r}_1,t)$ with the initial condition,

$$P(\mathbf{r}_0,\mathbf{r}_1,0) = \delta(\mathbf{r}_1 - \mathbf{r}_0) \qquad [25]$$

(n.b., δ in Eq. [25] is the Dirac delta function, not the length of the gradient pulse). Thus, if in Eq. [18] $P(\mathbf{r}_0,\mathbf{r}_1,t)$ is substituted for $c(\mathbf{r},t)$, $\mathbf{J}$ becomes the conditional probability flux. Similarly, in terms of $P(\mathbf{r}_0,\mathbf{r}_1,t)$ Eq. [20] becomes

$$\frac{\partial P(\mathbf{r}_0,\mathbf{r}_1,t)}{\partial t} = D\nabla^2 P(\mathbf{r}_0,\mathbf{r}_1,t). \qquad [26]$$

In the case of anisotropic diffusion, Eq. [26] can be changed similarly to Eq. [23]. $P(\mathbf{r}_0,\mathbf{r}_1,t)$ is commonly termed the Green's function or diffusion propagator (*55, 63*).

For the case of (three-dimensional) diffusion in an isotropic and homogeneous medium (i.e., boundary condition $P \to 0$ as $\mathbf{r}_1 \to \infty$), $P(\mathbf{r}_0, \mathbf{r}_1, t)$ can determined from Eq. [26] using Fourier transforms (*64*) and is given by (*62*)

$$P(\mathbf{r}_0, \mathbf{r}_1, t) = (4\pi Dt)^{-3/2} \exp\left(-\frac{(\mathbf{r}_1 - \mathbf{r}_0)^2}{4Dt} \right). \quad [27]$$

Equation [27] states that the radial distribution function of the spins in an infinitely large system with regard to an arbitrary reference time is Gaussian. We note from Eq. [27] that $P(\mathbf{r}_0, \mathbf{r}_1, t)$ does not depend on the initial position, $\mathbf{r}_0$, but depends only on the net displacement, $\mathbf{r}_1 - \mathbf{r}_0$ (the vector $\mathbf{r}_1 - \mathbf{r}_0$ moved during time t is often referred to as the dynamic displacement $\mathbf{R}$). This reflects the Markovian nature (*10, 65*) of Brownian motion. The solution of Eq. [26] becomes much more complicated when the displacement of the particle is affected by its boundaries (e.g., diffusion in a sphere) and $P(\mathbf{r}_0, \mathbf{r}_1, t)$ is no longer Gaussian. The solutions of Eq. [26] for many cases of interest can be found in the literature (*62, 66*). It should be noted that the mathematics of heat conduction, after making the appropriate changes of notation, is identical to that for describing diffusion (*62*).

It is an appropriate stage to consider the $\rho(\mathbf{r}_0)$, the probability that a spin starts at $\mathbf{r}_0$, in some detail. Formally, $\rho(\mathbf{r}_0)$ is given by

$$\rho(\mathbf{r}_0) = \int \lim_{t \to \infty} P(\mathbf{r}_0, \mathbf{r}_1, t)\, d\mathbf{r}_1 \quad [28]$$

and thus is independent of $\mathbf{r}_0$, because after infinite time the finishing position of a particle in the system will be independent of the starting position. $P(\mathbf{r}_0, \mathbf{r}_1, t)$ as given by Eq. [27] (i.e., free diffusion) approaches 0 as $t \to \infty$, but the "effective volume" (i.e., the integral over $\mathbf{r}_1$) becomes proportionally larger; consequently, $\rho(\mathbf{r}_0)$ stays constant (1 is a convenient choice). In the case of an enclosed geometry, $\rho(\mathbf{r}_0)$ is given by the inverse of the volume. Also, by definition we must have [e.g., ref. (*65*)]

$$\int \rho(\mathbf{r}_0)\, d\mathbf{r}_0 = 1. \quad [29]$$

The mean-squared displacement is given by [e.g., Ref. (*10*)]

$$\left\langle (r_1 - r_0)^2 \right\rangle = \int_{-\infty}^{\infty} (\mathbf{r}_1 - \mathbf{r}_0)^2 \rho(\mathbf{r}_0) P(\mathbf{r}_0, \mathbf{r}_1, t)\, d\mathbf{r}_0\, d\mathbf{r}_1. \quad [30]$$

Using $P(\mathbf{r}_0, \mathbf{r}_1, t)$ as given by Eq. [27], we can calculate the mean-squared displacement of free diffusion. To do this we rewrite Eq. [27] in Cartesian form (i.e., $\mathbf{r} = x\mathbf{i} + y\mathbf{j} + z\mathbf{k}$)

$$P(\mathbf{r}_0, \mathbf{r}_1, t) = (4\pi Dt)^{-3/2} \exp\left(-\frac{(x_1 - x_0)^2}{4Dt} \right) \times \exp\left(-\frac{(y_1 - y_0)^2}{4Dt} \right) \times \exp\left(-\frac{(z_1 - z_0)^2}{4Dt} \right) \quad [31]$$

and using Eq. [30] and noting that $\rho(\mathbf{r}_0) = 1$ for the case of free diffusion. We can evaluate Eq. [30] using the standard integral [e.g., Eq. 3.462 8. in Ref. (*53*)],

$$\int_{-\infty}^{\infty} x^2 e^{-\mu x^2 + 2\nu x}\, dx = \frac{1}{2\mu}\sqrt{\frac{\pi}{\mu}}\left(1 + 2\frac{\nu^2}{\mu}\right) e^{\nu^2/\mu} \quad [|\arg \nu| < \pi, \operatorname{Re}\mu > 0] \quad [32]$$

where in our case $x = x_1 - x_0, y_1 - y_0, z_1 - z_0$, $\mu = (4Dt)^{-1}$ and $\nu = 0$, and thus we obtain (n.b. for free diffusion)

$$\left\langle (r_1 - r_0)^2 \right\rangle = nDt \quad [33]$$

where $n = 2, 4$, or 6 for one, two, or three dimensions, respectively. Equation [30] presents a relationship between the molecular displacement due to diffusion and the diffusion equation. Specifically for free diffusion, it states that the mean-squared displacement changes linearly with time.

When we use the PFG method to measure diffusion in free solution and in the absence of exchange, the length of time we choose (i.e., Δ) is irrelevant and we get the same result (i.e., from Eq. [33] the mean-squared displacement scales linearly with time). This is, of course, assuming that the relaxation time(s) of the species in question is sufficiently long so that we still get a measurable signal and that the measurement is unaffected by eddy currents or other experimental complications [see, for example, ref. (*19*)]. However, in the case of a species diffusing within a confined space we must be careful to properly account for the effects of the restricting geometry on the motion of the species. If a particle is diffusing within a restricted geometry (sometimes referred to as a "pore"), the displacement along the z-axis will be a function of Δ, the diffusion coefficient, and the size and shape of the restricting geometry. Consequently, if the boundary effects are not properly accounted for and we analyze the data using the model for free diffusion (see the next section), we will measure an apparent diffusion coefficient (D_{app}) and not the true diffusion coefficient. We illustrate this effect later in this section.

Before further considering the problem of restricted diffusion, it is appropriate to briefly consider what constitutes the true diffusion coefficient. In a pure liquid (e.g., water) the true diffusion coefficient corresponds to the bulk diffusion coefficient. However, the situation is rather more complex in a macromolecular solution (e.g., cell cytoplasm, polymer solutions, protein solutions, etc.) where the probe molecule (e.g., water) has to skirt around the larger "obstructing" molecules (e.g., proteins, organelles) as well as perhaps interacting with protein hydration shells [e.g., Ref. (*67*)]. These effects operate on a time scale much smaller than the smallest experimentally available Δ and consequently are well averaged on the time scale of Δ. For example, if we consider a reasonably small value of Δ of 5 ms and that at 298 K water has a diffusion coefficient of about 2.3×10^{-9} m^{2}s^{-1} (*68, 69*), then from Eq. [30] the mean displacement of a water molecule during Δ is about 5 μm. The true diffusion coefficient will be an average bulk diffusion coefficient consisting of all of the interactions that affect the probe molecule diffusion. The situation can be further complicated by the effects of exchange through cell membranes (*70*). The different time scales of the averaging processes is one of the major reasons that diffusion probed by using relaxation studies and diffusion measured using PFG NMR are essentially different things with the relaxation based measurements probing motion on the time scale of the correlation time of the probe molecule and not on the (much longer) time scale of Δ (*21, 71*). We mention in passing that in a polymer solution if the diffusion of the polymer itself is studied there can be additional complications owing to the entanglement of the polymer molecules [e.g., Ref (*19*) and references therein].

We now explain the concept of restricted diffusion and how it relates to PFG NMR diffusion measurements. Consider two cases where we have a particle with the same diffusion coefficient; in one case the particle is freely diffusing (i.e., an isotropic homogeneous system), while in the other case it is confined to a reflecting sphere of radius R (Fig. 4). By "reflecting" we mean that the spin is neither transported through the boundary nor relaxed by the contact with the boundary. From Eq. [30], we can define the dimensionless variable (i.e., $n = 1$, $t = \Delta$),

$$\xi = D\Delta/R^2, \qquad [34]$$

which is useful in characterizing restricted diffusion as will be seen below. In the case of freely diffusing particles, the diffusion coefficient determined will be independent of Δ and the displacement measured in the z-direction will reflect the true diffusion coefficient, since the mean-squared displacement scales linearly with time (see Eq. [33]). However, for the particle confined to the sphere, the situation is entirely different. For short values of Δ such that the diffusing particle has not diffused far enough to feel the effect of the boundary (i.e., $\xi \ll 1$), the measured diffusion coefficient will be the same as that observed for the freely diffusing species. As Δ becomes finite (i.e., $\xi \approx 1$), a certain fraction of the particles (i.e., in a real NMR experiment there is an ensemble of diffusing species) will feel the effects of the boundary and the mean squared displacement along the z-axis will not scale linearly with Δ; thus, the measured diffusion coefficient (i.e., D_{app}) will appear to be (observation) time dependent. At very long Δ, the maximum distance that the confined particle can travel is limited by the boundaries, and thus the measured mean-squared displacement and diffusion coefficient becomes independent of Δ. Thus, for short values of Δ the measured displacement of a particle in a restricting geometry observed via the signal attenuation in the PFG experiment is sensitive to the diffusion of the particle. At long Δ the signal attenuation becomes sensitive to the shape and dimensions of the restricting geometry. The relationships between the experimental parameters are further examined in the next section. If the restricting geometry is spherically symmetric, then there will be no-orientational dependence with

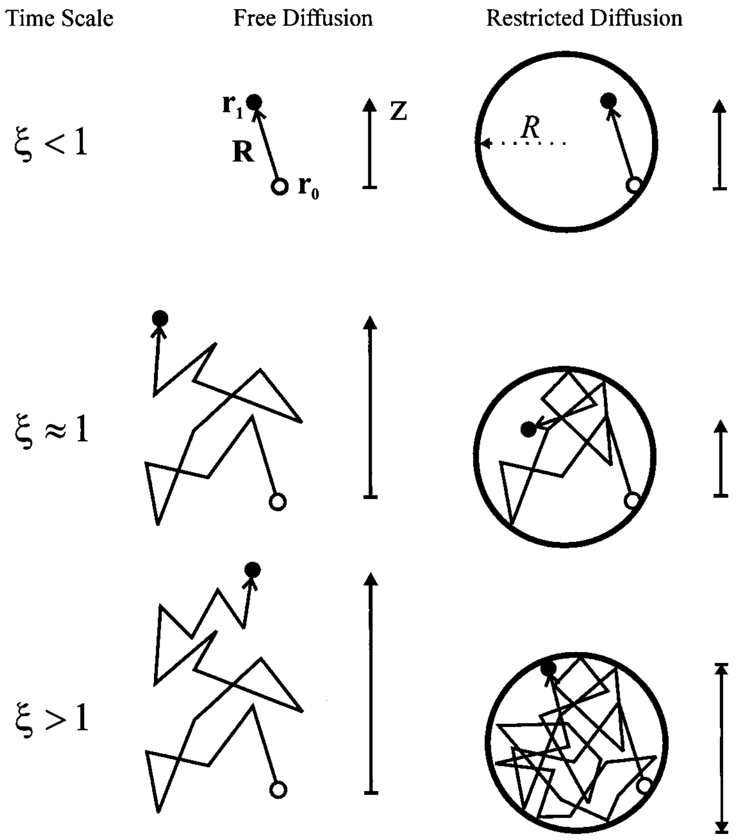

Figure 4 In the PFG experiment, we use the first gradient pulse to label the starting position of the diffusing species and the second gradient pulse, at a time Δ later, to probe its finishing position with respect to the gradient direction. The important point is that we do not know what happens between these two times. In this diagram we schematically represent what happens when we measure the diffusion coefficient of a species when it is undergoing free diffusion or restricted diffusion in a sphere of radius R. $\mathbf{r}_0$ denotes the starting position (○), and $\mathbf{r}_1$ denotes the position (●) at a time Δ later. The length of the arrows (i.e., **R**) denote the measured displacement in the direction of the gradient which is normally in the z direction and is taken to be up the page in the present diagram. We consider three relevant time scales for the measurement of the effects of the restricted diffusion; (i) ξ $(= D\Delta/R^2)$ $\ll 1$ (the short time limit); the particle does not diffuse far enough during Δ to feel the effects of restriction. Measurements performed within this time scale lead to the true diffusion coefficient (i.e., D). (ii) $\xi \approx 1$; some of the particles feel the effects of restriction and the diffusion coefficient measured within this time scale will be apparent (i.e., D_{app}) and be a function of Δ. The fraction of particles that feel the effects of the boundary will be dependent on the surface-to-volume ratio S_{geo}/V. (iii) $\xi > 1$ (the long time limit); all particles feel the effects of restriction. In this time scale, the displacement of the particle is independent of Δ and depends only on R. Thus, restriction causes a (measuring-time)-dependent diffusion coefficient in which at Δ the displacement is limited by the embedding geometry.

respect to the gradient direction of the measured displacement. However, particularly in *in vivo* systems (e.g., muscle cells), where the restricting geometry is normally not spherically symmetric, and in liquid crystals where the diffusion can be anisotropic, the observed signal attenuation will have an orientational dependence. This aspect will be considered subsequently.

We should also mention that "obstruction" can be thought of as a type of restricted diffusion. The change in the diffusion coefficient due to obstruction is a source of information on the shape of the obstructing particle, e.g., Refs. (*72–74*). The mathematical description of obstruction effects is very difficult, since the diffusion path of the probe molecule can be very complicated; also the obstructing particles are not (necessarily) distributed in space in a totally ordered or totally random way.

CORRELATING SIGNAL ATTENUATION WITH DIFFUSION

Introduction

We will now discuss the mathematical formulations necessary to relate the signal attenuation to the diffusion coefficient and boundary conditions in the PFG experiment. Starting from the Bloch equations modified to include the diffusion of magnetization (*75, 76*) it is possible to derive the necessary relationships analytically for free diffusion, as we shall show below. However, in the case of restricted diffusion this macroscopic approachbecomes mathematically intractable. Thus, in general case one is forced to use different approximations to find formulae relating E to the diffusion coefficient, boundary, and experimental conditions. There are two common approximations, namely: the GPD approximation and the SGP approximation. However, even using these approximations, analytic solutions are generally not possible and numerical methods must be used. In this section, we will only consider the case of free diffusion and describe the macroscopic approach and the SGP and GPD approximations in this case. It is assumed that the gradient pulses are rectangular. Detailed discussion of the signal attenuation of spins undergoing restricted diffusion will be deferred until later in this section.

The Macroscopic Approach

Bloch Equations Including the Effects of Diffusion. The Bloch equations for the macroscopic nuclear magnetization, $\mathbf{M}(\mathbf{r},t) = M_x + M_y + M_z$, including the diffusion of magnetization, are given by (*75, 76*),

$$\frac{\partial \mathbf{M}(\mathbf{r},t)}{\partial t} = \gamma \mathbf{M} \times \mathbf{B}(\mathbf{r},t) - \frac{M_x \mathbf{i} + M_y \mathbf{j}}{T_2} - \frac{(M_z - M_0)\mathbf{k}}{T_1} + D\nabla^2 \mathbf{M}. \quad [35]$$

In the case of anisotropic diffusion, the last term in Eq. [35] would be replaced by $\nabla \cdot \mathbf{D} \cdot \nabla \mathbf{M}$. If we now take (as is usually the case) $\mathbf{B}_0$ to be oriented along the z-axis and that this is superposed by a gradient $\mathbf{g}$ vanishing at the origin which is parallel to $\mathbf{B}_0$ (we assume that the inhomogeneities caused by $\mathbf{g}$ are much smaller than $\mathbf{B}_0$), and thus we can write

$$B_x = 0, \quad B_y = 0,$$

$$B_z = B_0 + (\mathbf{g} \cdot \mathbf{r}) = B_0 + g_x x + g_y y + g_z z \quad [36]$$

If Eq. [36] is then substituted into Eq. [35], noting that

$$\mathbf{M} \times \mathbf{B} = (M_y B_z - M_z B_y)_x + (M_z B_x - M_x B_z)_y + (M_x B_y - M_y B_x)_z \quad [37]$$

and defining the (complex) transverse magnetization as

$$m = M_x + iM_y \quad [38]$$

we obtain

$$\frac{\partial m}{\partial t} = -i\omega_0 m - i\gamma(\mathbf{g} \cdot \mathbf{r})m - m/T_2 + D\nabla^2 m. \quad [39]$$

The Stejskal and Tanner Pulse Sequence in the Absence of Diffusion. In the absence of diffusion (i.e., $D = 0$), m relaxes exponentially with a time constant T_2, and thus we set

$$m = \psi e^{-i\omega_0 t - t/T_2} \quad [40]$$

where ψ represents the amplitude of the precessing magnetization unaffected by the effects of relaxation. If we substitute Eq. [40] into [39], we obtain

$$\frac{\partial \psi}{\partial t} = -i\gamma(\mathbf{g} \cdot \mathbf{r})\psi + D\nabla^2 \psi. \quad [41]$$

In the absence of diffusion, Eq. [41] is a first-order ordinary differential equation with solution

$$\psi(r,t) = S \exp(-i\gamma \mathbf{r} \cdot \mathbf{F}) \quad [42]$$

where S is a constant and

$$\mathbf{F}(t) = \int_0^t \mathbf{g}(t')\,dt'. \quad [43]$$

Now, if we consider the case of the PFG pulse sequence, then during the period from the $\pi/2$ pulse to the π pulse, we have (i.e., Eq. [42])

$$\psi(r,t) = S \exp(-i\gamma \mathbf{r} \cdot \mathbf{F}), \quad [44]$$

and S corresponds to the value of ψ immediately after the $\pi/2$ pulse. After the π pulse (neglecting the phase angle of the π pulse, which is of no consequence here), we have

$$\psi(r,t) = S\exp(-i\gamma\mathbf{r}\cdot(\mathbf{F} - 2\mathbf{f})), \qquad [45]$$

where

$$\mathbf{f} = \mathbf{F}(\tau). \qquad [46]$$

Thus, from Eq. [45] we can see that the effect of the π pulse is to set back the phase of ψ by twice the amount that it had advanced up until the π pulse (see the first series of phase diagrams in Fig. 2). Equations [44] and [45] can then be combined into

$$\psi(r,t) = S\exp(-i\gamma\mathbf{r}\cdot(\mathbf{F} - 2H(t-\tau)\mathbf{f})) \qquad [47]$$

where $H(t)$ is the Heaviside step function. We note here that Eq. [47] is valid for the Hahn spin-echo pulse sequence.

The Stejskal and Tanner Pulse Sequence in the Presence of Diffusion. In the previous section, we considered the solution to Eq. [41] in the absence of the diffusion. In this section, we derive a solution to Eq. [41] including the effects of diffusion. We assume a solution to Eq. [41], including the diffusion term, to be of the form of Eq. [47] but allow S to be a function of t [i.e., $S(t)$]. By substituting Eq. [47] into Eq. [41], we obtain

$$\frac{dS(t)}{dt} = -\gamma^2 D[\mathbf{F} - 2H(t-\tau)\mathbf{f}]^2 S(t) \qquad [48]$$

Now we integrate Eq. [48] from $t = 0$ to $t = 2\tau$

$$\begin{aligned}\ln\left[\frac{S(2\tau)}{S(0)}\right] &= \ln(E(2\tau))\\ &= \int_0^{\tau} -\gamma^2 D\mathbf{F}^2\,dt + \int_{\tau}^{2\tau} -\gamma^2 D[\mathbf{F} - 2\mathbf{f}]^2\,dt\\ &= -\gamma^2 D\left\{\int_0^{2\tau} F^2\,dt - 4\mathbf{f}\int_{\tau}^{2\tau}\mathbf{F}\,dt + 4f^2\tau\right\}\end{aligned} \qquad [49]$$

The application of Eq. [49] to the calculation of the echo attenuation resulting from the effects of diffusion and the application of gradients is quite straightforward but rather tedious. If we apply the gradient pulses as shown in the pulse sequences in Fig. 2 and neglect the effects of any background gradients, then we can define $\mathbf{g}(t)$ and the effective field gradient, $\mathbf{g}_{eff}(t)$, as in Table 1. It is important to note that the lower limit of integration in Eq. [43] refers to the start of the sequence. For example, using the above definition of $\mathbf{g}(t)$, $F(t)$ for $t_1 + \Delta < t \le t_1 + \Delta + \delta$ is calculated as follows,

$$\begin{aligned}F(t) &= \int_0^{t_1} 0\,dt + \int_{t_1}^{t_1+\delta} g\,dt\\ &\quad + \int_{t_1+\delta}^{t_1+\Delta} 0\,dt + \int_{t_1+\Delta}^{t} g\,dt\\ &= g(t + \delta - t_1 - \Delta).\end{aligned} \qquad [50]$$

An example of the use of the symbolic algebra package Maple (*77*) to calculate Eq. [49] is given in the Appendix, and from this we obtain the result (*54*)

$$\ln(E) = -\gamma^2 g^2 D\delta^2(\Delta - \delta/3). \qquad [51]$$

The term $\delta/3$ accounts for the finite width of the gradient pulse. Equation [51] is not a function of t_1, and thus the placement of the gradient pulses in the sequence is of no consequence; for example, there is no requirement that the gradient pulses be symmetrically placed around the π pulse. If instead we had imposed a steady gradient throughout the echo sequence (i.e., $\Delta = \delta = \tau$), we would have reproduced the well-known diffusion term in the expression for the intensity of the Hahn spin-echo sequence (see Eq. [17]), as expected.

It is instructive to consider Eq. [51] in some detail. Let us suppose that we do an experiment at, say 298 K on a sample containing a small molecule, such as water, which has a diffusion coefficient of about 2.3×10^{-9} $\mathrm{m^2s^{-1}}$ (*68, 69*) and a protein with a diffusion coefficient of 1×10^{-10} $\mathrm{m^2s^{-1}}$. From our discussion above and also Eq. [51], it is apparent that after we have cali-

Table 1 $\mathbf{g}(t)$ and $\mathbf{g}_{\mathrm{eff}}(t)$ for the Stejskal and Tanner Pulse Sequence

Subinterval of Pulse Sequence	$\mathbf{g}(t)$	$\mathbf{g}_{eff}(t)$
$0 < t \le t_1$	0	0
$t_1 < t \le t_1 + \delta$	g	$-g$
$t_1 + \delta < t \le t_1 + \Delta$	0	0
$t_1 + \Delta < t \le t_1 + \Delta + \delta$	g	g
$t_1 + \Delta + \delta < t \le 2\tau$	0	0

brated the gradient and decided upon which nucleus we shall use to probe diffusion, we are left with three experimental variables to choose from (i.e., δ, Δ, or g). Increasing any of these three parameters will lead to increased signal attenuation, and is thus a means of measuring diffusion; for example, in Fig. 3 we altered δ. While we are free to choose which parameter we wish to vary, the relaxation characteristics of the sample and technical reasons may limit our choice. Some simulated "typical experimental results" for a PFG experiment on the water–protein solution are plotted in Fig. 5. This simple plot conveys a wealth of information. We have chosen to plot E on a log scale versus $\gamma^2 g^2 \delta^2(\Delta - \delta/3)$, and thus from Eq. [51] we see that each data set is a straight line with a slope given by $-D$, where D is the respective diffusion coefficient of the species in question. Of course, we could have just plotted our data against the experimental variable, but by using $\gamma^2 g^2 \Delta^2(\Delta - \delta/3)$ as the abscissa, data acquired using different experimental conditions are more easily compared. It can be clearly seen that as the diffusion coefficient decreases (i.e., larger molecule and/or more viscous solution), the slope decreases which experimentally is reflected by less attenuation.

In all of the discussion above, the gradient pulses have been taken to be rectangular. This is more out of technical and mathematical convenience than necessity. It should be mentioned that in the PEG experiment the gradient pulses do not have to be rectangular, and in fact to minimize the generation of eddy currents, it may be preferable to have nonrectangular pulses. Using Eq. [49], the effects of arbitrarily shaped gradient pulses can be considered (*78*) and the computations can be conveniently performed by simple modification of the Maple worksheet given in the Appendix. Another commonly used and totally equivalent means of solving Eq. [41] is to substitute Eq. [44], but where S is a function of t, into Eq. [41] directly and solving for S to obtain

$$\ln(E(t)) = -\gamma^2 D \int_0^t F^2\, dt. \qquad [52]$$

In evaluating Eq. [52], the applied field gradient must be replaced by the effective field gradient, $\mathbf{g}_{eff}$, such that the sign of the gradient is changed

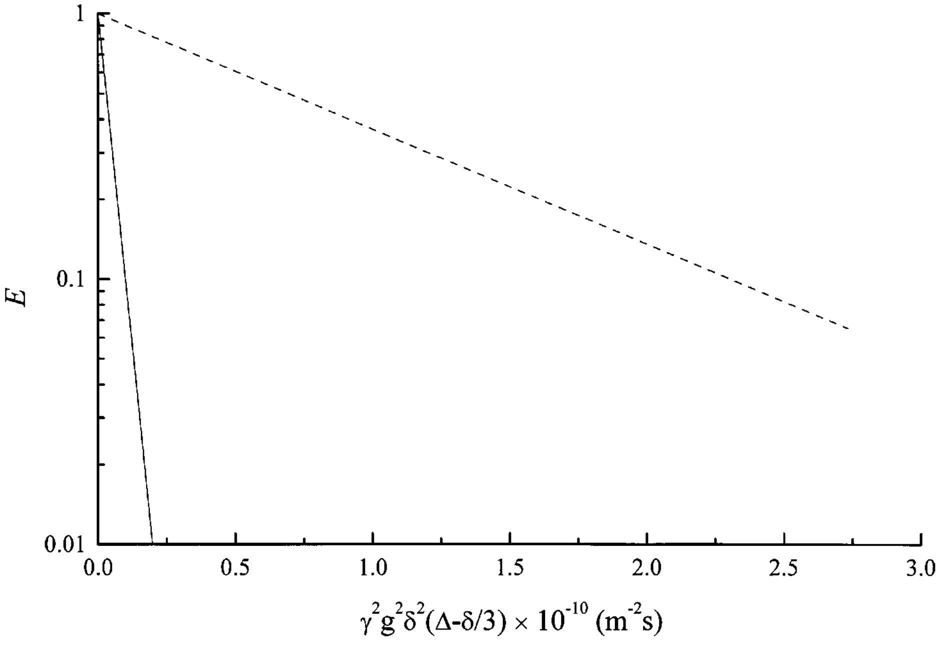

Figure 5 A plot of the simulated echo attenuation for determining the diffusion coefficient of water (——) and protein (- - -). The simulations were performed using Eq. [51] with $\gamma = \gamma^{^1H} = 2.6571 \times 10^8$ rad T^{-1}s^{-1}, $g = 0.2$ T m^{-1}, $\Delta = 100$ ms, and δ ranging from 0 to 10 ms. The diffusion coefficient of water and the protein were taken to be 2.33×10^{-9} and 1×10^{-10} m^{2}s^{-1}, respectively. As the diffusion coefficient increases, the slope of the line increases. If $\ln(E)$ is plotted on a linear scale versus the same abscissa the slope is given by $-D$ (see Eq. [51]).

every time a π pulse is applied. Thus, if Eq. [52] is used to evaluate the PFG pulse sequence, $\mathbf{g}_{eff}$ is used as defined above and the final results is, as before, given by Eq. [51]. Sometimes, especially in clinically oriented literature, Eq. [52] is written as

$$\ln(E(t)) = -bD \qquad [53]$$

where the "gradient" or "diffusion weighting" factor b is defined by

$$b = \gamma^2 \int_0^t F^2\,dt. \qquad [54]$$

Of course, for the Stejskal and Tanner sequence, in the case of free diffusion, $b = \gamma^2 g^2 \delta^2 (\Delta - \delta/3)$.

Although only isotropic diffusion was considered in this section, and therefore we used a scalar diffusion coefficient, D, the derivations could equally well have been performed for anisotropic diffusion using the diffusion tensor $\mathbf{D}$. This is considered in detail later.

The Stejskal and Tanner Pulse Sequence in the Presence of Diffusion and Flow. If Eq. [35] is supplemented with a term reflecting flow (i.e., $-\nabla \mathbf{v} M$) where $\mathbf{v}$ is the velocity of the medium in which the spins are in and similar analysis is carried out as above, then we get, assuming flow along the direction of gradient, (55)

$$\ln(E) = \underbrace{-\gamma^2 g^2 D \delta^2 (\Delta - \delta/3)}_{\text{attenuation}} + \underbrace{i\gamma\delta g\Delta v}_{\text{net phase change}} \quad . \qquad [55]$$

We note that whereas diffusion results in a loss of echo intensity, flow causes a net phase shift (n.b., the complex "i"). This is depicted in the third series of phase diagrams in Fig. 2.

The GPD Approximation

In this section, the first of the two common approximations used to relate the echo-signal attenuation to the diffusion coefficient and the experimental variables is introduced. In the second section it was shown that the echo-signal attenuation could be defined as (i.e., Eq. [12])

$$S(2\tau) = S(2\tau)_{g=0} \int_{-\infty}^{\infty} P(\phi, 2\tau) \cos\phi \, d\phi$$

with ϕ being defined by (Eq. [9]) $\phi_i(2\tau) = \gamma g\{\int_{t_1}^{t_1+\delta} z_i(t)\,dt - \int_{t_1+\Delta}^{t_1+\Delta+\delta} z_i(t')\,dt'\}$. We need to derive $P(\phi, 2\tau)$ from Eq. [9]. We begin by noting that $z_i(t)$ is described by the one-dimensional diffusion equation which is a Gaussian for the case of unbounded diffusion (i.e., the one-dimensional version of Eq. [27], i.e., start with Eq. [31] and integrate over the x and y coordinates using Eq. [64] below),

$$P(0, z, t) = (4\pi D t)^{-1/2} \exp\left(\frac{-z^2}{4Dt} \right). \qquad [56]$$

Now as the probability density for the integral of a variable [in the present case $z_i(t)$], which itself has a Gaussian probability density, is Gaussian [e.g., see Ref. (65)], we have

$$P(\phi, 2\tau) = (2\pi \langle \phi^2 \rangle_{av})^{-1/2} \exp\left(\frac{-\phi^2}{2\langle \phi^2 \rangle_{av}} \right) \qquad [57]$$

where $\langle \phi^2 \rangle$ is the mean-squared phase change at $t = 2\tau$, which is given by

$$\langle \phi^2 \rangle_{av} = \gamma^2 g^2 \left\langle \left\{ \int_{t_1}^{t_1+\delta} z_i(t)\,dt - \int_{t_1+\Delta}^{t_1+\Delta+\delta} z_i(t)\,dt \right\}^2 \right\rangle_{av}. \qquad [58]$$

To avoid confusion with t, we use t_a and t_b as our dummy variables of integration, and thus, Eq. [58] becomes

$$\begin{aligned} \langle \phi^2 \rangle_{av} = \gamma^2 g^2 \Bigg\{ & \int_{t_1}^{t_1+\delta} \int_{t_1}^{t_1+\delta} dt_a\,dt_b \\ & - 2\int_{t_1}^{t_1+\delta} \int_{t_1+\Delta}^{t_1+\Delta+\delta} dt_a\,dt_b \\ & + \int_{t_1+\Delta}^{t_1+\Delta+\delta} \int_{t_1+\Delta}^{t_1+\Delta+\delta} dt_a\,dt_b \Bigg\} \\ & \times \langle z(t_a) z(t_b) \rangle_{av}. \end{aligned} \qquad [59]$$

From Eq. [59], we see that the computation of $\langle \phi^2 \rangle$ can be separated into two pieces: a spatial part given by the mean-squared displacement in the direction of the gradient, $\langle z(t_a) z(t_b) \rangle_{av}$, and a temporal part (i.e., the time integrals). Thus, we first need to calculate $\langle z(t_a) z(t_b) \rangle_{av}$. We need to express $\langle z(t_a) z(t_b) \rangle_{av}$ as the products of the probability of each motion times the corresponding displacement in the direction of the gradient, which can be written most generally as (*79*)

$$\langle z(t_a)z(t_b)\rangle_{av} = \iiint(\mathbf{r}_1-\mathbf{r}_0)_z(\mathbf{r}_2-\mathbf{r}_0)_z\rho(\mathbf{r}_0)P(\mathbf{r}_0,\mathbf{r}_1,t_a) \times P(\mathbf{r}_1,\mathbf{r}_2,t_b-t_a)\,d\mathbf{r}_0\,d\mathbf{r}_1\,d\mathbf{r}_2. \qquad [60]$$

It should be noted that Eq. [60] holds only when $t_b > t_a$. We will now evaluate Eq. [60] for the (particularly simple) case of $P(\mathbf{r}_0, \mathbf{r}_1, t)$ as given by Eq. [27] (i.e., free diffusion). Since we are only interested in motion in one dimension, we can simplify our task by using the one-dimensional version of Eq. [27],

$$P(z_0,z_1,t) = (4\pi Dt)^{-1/2}\exp\left(-\frac{(z_1-z_0)^2}{4Dt}\right) \qquad [61]$$

and making obvious changes to Eq. [60] thus obtain

$$\langle z(t_a)z(t_b)\rangle_{av} = \int_{-\infty}^{\infty}\int_{-\infty}^{\infty}\int_{-\infty}^{\infty}\rho(z_0)(z_1-z_0)(z_2-z_0) \times(4\pi Dt_a)^{-1/2} \times\exp\left(-\frac{(z_1-z_0)^2}{4Dt_a}\right)(4\pi D(t_b-t_a))^{-1/2} \times\exp\left(-\frac{(z_2-z_1)^2}{4D(t_b-t_a)}\right)dz_0\,dz_1\,dz_2.$$

Now we let $Z_1 = z_1 - z_0$ and $Z_2 = z_2 - z_0$, and thus,

$$\int_{-\infty}^{\infty}\rho(z_0)\,dz_0 \times\int_{-\infty}^{\infty}Z_1(4\pi Dt_a)^{-1/2}\exp\left(-\frac{Z_1^2}{4Dt_a}\right)dZ_1 \times\int_{-\infty}^{\infty}Z_2(4\pi D(t_b-t_a))^{-1/2} \times\exp\left(-\frac{(Z_2-Z_1)^2}{4D(t_b-t_a)}\right)dZ_2.$$

By noting Eq. [29], we can remove the integral over z_0, and making the substitution $Z_2' = Z_2 - Z_1$, we then get

$$\int_{-\infty}^{\infty}Z_1(4\pi Dt_a)^{-1/2}\exp\left(-\frac{Z_1^2}{4Dt_a}\right)dZ_1 \times\int_{-\infty}^{\infty}(Z_2'+Z_1)(4\pi D(t_b-t_a))^{-1/2} \times\exp\left(-\frac{Z_2'^2}{4D(t_b-t_a)}\right)dZ_2'. \qquad [62]$$

We now consider the integral over Z_2' in Eq. [62], which we rewrite as

$$(4\pi D(t_b-t_a))^{-1/2} \times\left\{Z_1\int_{-\infty}^{\infty}\exp\left(-\frac{Z_2'^2}{4D(t_b-t_a)}\right)dZ' +\int_{-\infty}^{\infty}Z_2'\exp\left(-\frac{Z_2'^2}{4D(t_b-t_a)}\right)dZ'\right\}. \qquad [63]$$

The first integral in Eq. [63] can be evaluated with the standard integral [e.g., integral 3.323 2. in Ref. (*53*)],

$$\int_{-\infty}^{\infty}e^{-p^2x^2\pm qx}\,dx = e^{q^2/4p^2}\frac{\sqrt{\pi}}{|p|}. \qquad [64]$$

by setting $x = Z_2'$, $p = (4D(t_a - t_b))^{-1/2}$ and $q = 0$, to give $(4\pi D(t_b - t_a))^{1/2}$. The second integral in Eq. [63] can be evaluated using the standard integral [Eq. 3.462 6. in Ref. (*53*)],

$$\int_{-\infty}^{\infty}xe^{-px^2+2qx}\,dx = \frac{q}{p}\sqrt{\frac{\pi}{p}}\,e^{q^2/p^2} \quad [\operatorname{Re} p > 0]. \qquad [65]$$

In our case, $x = Z_2', p = 4D(t_b - t_a)$ and $q = 0$, and so this integral equals 0. Hence, Eq. [63] reduces to simply Z_1 and now Eq. [62] becomes

$$\langle z(t_a)z(t_b)\rangle_{av} = \int_{-\infty}^{\infty}Z_1^2(4\pi Dt_a)^{-1/2} \times\exp\left(-\frac{Z_1^2}{4Dt_a}\right)dZ_1. \qquad [66]$$

Finally, noting the standard integral given in Eq. [32], we obtain the final result of

$$\langle z(t_a)z(t_b)\rangle_{av} = 2Dt_a \qquad [67]$$

which is of course equal to the mean-squared displacement for the one-dimensional diffusion equation (see Eq. [30]).

We now come to a subtle point in evaluating Eqs. [59] and [60]. In performing the integrals, we need to consider the range of integration when inputting $\langle z(t_a)z(t_b)\rangle_{av}$; that is, we have to interchange t_a for t_b in Eq. [60] depending on whether $t_a > t_b$ or $t_a < t_b$. This can be understood by noting that the exponentials in Eq. [60] must have negative exponents (recall the validity of Eq. [60]); hence, we get *(60, 80)*

$$\begin{aligned}\langle z(t_a)z(t_b)\rangle_{av} &= \langle z^2(t_a)\rangle_{av} = 2Dt_a \text{ if } t_a < t_b\\ \langle z(t_a)z(t_b)\rangle_{av} &= \langle z^2(t_b)\rangle_{av} = 2Dt_b \text{ if } t_a > t_b.\end{aligned} \qquad [68]$$

Continuing on with our derivation of Eq. [58], we have

$$\begin{aligned}\langle\phi^2\rangle_{av} = \gamma^2 g^2\Bigg\{&\int_{t_1}^{t_1+\delta}\left[\int_{t_1}^{t_a} 2Dt_b\,dt_b + \int_{t_a}^{t_1+\delta} 2Dt_a\,dt_b\right]dt_a\\ &-2\int_{t_1}^{t_1+\delta}\int_{t_1+\Delta}^{t_1+\Delta+\delta} 2Dt_a\,dt_b\,dt_a\\ &+\int_{t_1+\Delta}^{t_1+\Delta+\delta}\left[\int_{t_1+\Delta}^{t_a} 2Dt_b\,dt_b + \int_{t_a}^{t_1+\Delta+\delta} 2Dt_a\,dt_b\right]dt_a\Bigg\}\\ = \gamma^2 g^2 2\delta^2(\Delta - \delta/3)&\end{aligned} \qquad [69]$$

If we evaluate Eq. [12] using the distribution of phases as given in Eq. [57], we find that the echo attenuation is given by

$$E = \exp(-\langle\phi^2\rangle/2). \qquad [70]$$

Finally, if we substitute Eq. [69] into Eq. [70], we get our final result (i.e., Eq. [51]) as before,

$$\ln(E) = -\gamma^2 g^2 D\delta^2(\Delta - \delta/3).$$

As expected, if we modify the limits of integration in Eq. [59], then the GPD approximation can be used to calculate the diffusion term in the expression for the intensity of the Hahn spin-echo sequence (see Eq. [17]) *(60, 80)*.

We have shown in this section that since the mean-squared phase change (i.e., $\langle\phi^2\rangle$) can be calculated exactly for unrestricted diffusion, the GPD approximation gives the same result as the macroscopic approach (i.e., Eq. [51]). Subsequently, the validity of the GPD approximation represented by Eq. [57] and its ramifications when the diffusion is bounded will be considered further.

SGP Approximation

To understand the SGP approximation, we start back at Eq. [7] but ignore the effects of motion during the gradient pulse (rigorously, one assumes that the gradient pulse is like a delta function, that is, $\delta \to 0$ and $|\mathbf{g}| \to \infty$, while their product remains finite). Experimentally, this condition is approximated by keeping $\delta \ll \Delta$. Hence, the effect of a gradient pulse of duration δ on a spin at position $\mathbf{r}$ is given by, neglecting the effect of the static field,

$$\phi(\mathbf{r}) = \gamma\delta\mathbf{g}\cdot\mathbf{r}. \qquad [71]$$

The scalar product arises because only motion parallel to the direction of the gradient will cause a change in the phase of the spin. Hence, if we consider the phase change of a spin which was at position $\mathbf{r}_0$ during the first gradient pulse and at position $\mathbf{r}_1$ during the second, then the change in phase in moving from $\mathbf{r}_0$ to $\mathbf{r}_1$ is given by

$$\Delta\phi(\mathbf{r}_1 - \mathbf{r}_0) = \gamma\delta\mathbf{g}\cdot(\mathbf{r}_1 - \mathbf{r}_0). \qquad [72]$$

(n.b., the Δ in Eq. [72] represents the difference in ϕ, not the duration between gradient pulses). Now we need to consider the probability of a spin starting at $\mathbf{r}_0$ (i.e., the starting spin density) at $t = 0$, $\rho(\mathbf{r}_0, 0)$, which is usually taken as being equal to the equilibrium spin density $\rho(\mathbf{r}_0)$ (see Eq. [28]). This assumption requires that insignificant relaxation occur between the first rf pulse (i.e., excitation) and the first gradient pulse. In practice this is normally the case. Now the probability of moving from $\mathbf{r}_0$ to $\mathbf{r}_1$ in time Δ (i.e., the separation between the gradient pulses) is, of course, given by $P(\mathbf{r}_0, \mathbf{r}_1, t)$ as before. Thus, the probability of a spin starting from $\mathbf{r}_0$ and moving to $\mathbf{r}_1$ in time Δ is given by (recall Eq. [24])

$$\rho(\mathbf{r}_0)P(\mathbf{r}_0,\mathbf{r}_1,\Delta). \qquad [73]$$

The NMR signal is proportional to the vector sum of the transverse components of the magnetization, and so the signal from one spin is given by

$$\rho(\mathbf{r}_0)P(\mathbf{r}_0,\mathbf{r}_1,\Delta)e^{i\gamma\delta\mathbf{g}\cdot(\mathbf{r}_1-\mathbf{r}_0)}. \qquad [74]$$

But in NMR, the signal results from the ensemble of spins, and thus we must integrate over all possible starting and finishing positions, and finally we arrive at our result (*55, 56*)

$$E(\mathbf{g},\Delta) = \iint \rho(\mathbf{r}_0)P(\mathbf{r}_0,\mathbf{r}_1,\Delta) \times e^{i\gamma\delta\mathbf{g}\cdot(\mathbf{r}_1-\mathbf{r}_0)}\,d\mathbf{r}_0\,d\mathbf{r}_1. \qquad [75]$$

Thus, the total signal is a superposition of signals (transverse magnetizations), in which each phase term is weighted by the probability for a spin to begin at $\mathbf{r}_0$ and move to $\mathbf{r}_1$ during Δ.

As an example, let us rederive Eq. [51] using the SGP approximation (i.e., Eq. [75]). From Eq. [75] and [27], we have

$$E(\mathbf{g},\Delta) = \iint \rho(\mathbf{r}_0)\frac{1}{(4\pi D\Delta)^{3/2}}\,e^{-(\mathbf{r}_1-\mathbf{r}_0)^2/4D\Delta} \times e^{i\gamma\delta\mathbf{g}\cdot(\mathbf{r}_1-\mathbf{r}_0)}\,d\mathbf{r}_1\,d\mathbf{r}_0. \qquad [76]$$

In the present case, we set $\mathbf{g} = g_z$ (we will drop the subscript z, however), and $\mathbf{R} = \mathbf{r}_1 - \mathbf{r}_0$. Using spherical polar coordinates (i.e., R is the radius and θ and φ are the polar and azimuthal angles, respectively), we note that $d\mathbf{R} = R^2 \sin\theta\, dR\, d\theta\, d\varphi$; also, since θ is the angle between R and g we have

$$E(\mathbf{g},\Delta) = \frac{1}{(4\pi D\Delta)^{3/2}}\int_0^{2\pi} d\varphi \int_0^{\infty} e^{-R^2/4D\Delta}R^2 \times \int_0^{\pi} e^{i\gamma\delta gR\cos\theta}\sin\theta\,d\theta\,dR \qquad [77]$$

As there is no φ dependence, it can be integrated out

$$\frac{2\pi}{(4\pi D\Delta)^{3/2}}\int_0^{\infty} e^{-R^2/4D\Delta}\,R^2 \times \int_0^{\pi} e^{i\gamma\delta gR\cos\theta}\sin\theta\,d\theta\,dR \qquad [78]$$

then, by noting that $d\cos\theta = -\sin\theta\,d\theta$, we get

$$\frac{2\pi}{(4\pi D\Delta)^{3/2}}\int_0^{\infty} e^{-R^2/4D\Delta}\,R^2\int_{-1}^{1} e^{i\gamma\delta gR\theta}\,d\theta\,dR. \qquad [79]$$

The integral over θ is then performed and evaluated using Eq. [11], resulting in

$$\frac{4\pi}{\gamma\delta g(4\pi D\Delta)^{3/2}}\int_0^{\infty} R\,e^{-R^2/4D\Delta}\sin(\gamma\delta gR)\,dR \qquad [80]$$

We note from a table of standard integrals [e.g., (*53*) Eq. 3.952 1.] that

$$\int_0^{\infty} xe^{-p^2x^2}\sin(ax)\,dx = \frac{a\sqrt{\pi}}{4p^3}e^{-a^2/4p^2}. \qquad [81]$$

In our case, $x = R$, $p = (4D\Delta)^{-1/2}$, and $a = \gamma\delta g$, and thus we obtain the final result

$$E(g,\Delta) = \exp(-\gamma^2 g^2 D\delta^2\Delta). \qquad [82]$$

This is the same as Eq. [51], but in the limit of $\delta \to 0$; thus the $\delta/3$ term which accounts for the finite width of the gradient pulse is absent. When we consider restricted diffusion, the evaluation of Eq. [75] proceeds in exactly the same manner, except that we must substitute the relevant $\rho(\mathbf{r}_0)$ and $P(\mathbf{r}_0,\mathbf{r}_1,t)$. However, as the confining geometry becomes more complicated, so does the mathematical complexity.

The Analogy between PFG Measurements and Scattering. Returning back to the derivation of the SGP approximation, and in particular, Eq. [72], because we are using a constant (commonly termed "linear") gradient, what is important is not the actual starting and finishing positions of the spin but the net displacement between the two points in the direction of the gradient. As before, we can write $\mathbf{R} = \mathbf{r}_1 - \mathbf{r}_0$ and, analogously to Eq. [73], the probability that a particle that starts at $\mathbf{r}_0$ displacing a distance $\mathbf{R}$ during Δ is given by (recall Eq. [24])

$$\rho(\mathbf{r}_0)P(\mathbf{r}_0,\mathbf{r}_0+\mathbf{R},\Delta). \qquad [83]$$

Now, if we integrate Eq. [83] over all possible starting positions, we obtain the "average propagator." This is the probability, $\bar{P}(\mathbf{R}, \Delta)$, that a molecule at any starting position will displace by $\mathbf{R}$ during the period Δ (*12, 63*)

$$\bar{P}(\mathbf{R}, \Delta) = \int \rho(\mathbf{r}_0) P(\mathbf{r}_0, \mathbf{r}_0 + \mathbf{R}, \Delta)\, d\mathbf{r}_0. \quad [84]$$

Using Eq. [84], Eq. [75] can be rewritten as

$$E(\mathbf{q}, \Delta) = \int \bar{P}(\mathbf{R}, \Delta) e^{i\gamma\delta\mathbf{g}\cdot\mathbf{R}}\, d\mathbf{R}. \quad [85]$$

Thus, from Eq. [85] we can see that PFG NMR is sensitive to the average propagator $\bar{P}(\mathbf{R}, \Delta)$. It is convenient to include the effects of the gradient into the analysis by defining the parameter, $\mathbf{q}$, by (*81*)

$$\mathbf{q} = (2\pi)^{-1}\gamma\delta\mathbf{g}, \quad [86]$$

where $\mathbf{q}$ has units of m^{-1} (n.b., some authors use $\mathbf{k} = \gamma\delta\mathbf{g}$), and thus we can rewrite Eq. [85] as

$$E(\mathbf{q}, \Delta) = \int \bar{P}(\mathbf{R}, \Delta) e^{i2\pi\mathbf{q}\cdot\mathbf{R}}\, d\mathbf{R}. \quad [87]$$

Physical insight can be gained by noting from Eq. [87] that there is a Fourier relationship (*82, 83*) between $E(\mathbf{q}, \Delta)$ and $\bar{P}(\mathbf{R}, \Delta)$ (*63, 84, 85*); that is, the Fourier transform of $E(\mathbf{q}, \Delta)$ with respect to $\mathbf{q}$ returns an image of $\bar{P}(\mathbf{R}, \Delta)$. $\bar{P}(\mathbf{R}, \Delta)$ will be equivalent to $P(\mathbf{r}_0, \mathbf{r}_1, t)$ only when $P(\mathbf{r}_0, \mathbf{r}_1, t)$ is independent of the starting position $\mathbf{r}_0$. While this is true for free diffusion (see Eq. [27] and the discussion thereafter), it is not true in the case of restricted diffusion or diffusion in macroscopically heterogeneous systems. We can think of PFG diffusion measurements as $\mathbf{q}$-space imaging. From Eq. [86], we see that we can traverse $\mathbf{q}$-space by either changing δ or g, and we can change the direction by altering $\mathbf{g}$ (i.e., the direction of the gradient). Thus, PFG diffusion measurements are analogous to normal NMR imaging (also termed $\mathbf{k}$-space imaging) (*41, 42*), except that normal NMR imaging returns the spin density $\rho(\mathbf{r}_0)$. Or, to be more mathematically succinct, in PFG diffusion measurements $\mathbf{q}$-space is conjugate to $\mathbf{R}$, while in normal imaging $\mathbf{k}$-space is conjugate to $\mathbf{r}_0$.

Thus, Eq. [75] is analogous to the scattering function which applies in neutron scattering and $\mathbf{q}$ corresponds to the scattering wave vector (*41, 86, 87*). However, there are major differences in the temporal and spatial time scales of each type of experiment. Further, $E(\mathbf{q}, \Delta)$ is measured in the time domain of Δ in PFG experiments and in the frequency domain for neutron scattering experiments.

"Diffusive Diffraction" and Imaging Molecular Motion. Consider a spin trapped within a fully enclosed pore (e.g., a spin diffusing between parallel planes). In the long-time limit (i.e., $\Delta \to \infty$), all species lose memory of their starting position (i.e., they become independent of their starting position and, therefore, the diffusional process), and so

$$P(\mathbf{r}_0, \mathbf{r}_1, \infty) = \rho(\mathbf{r}_1) \quad [88]$$

and the average propagator becomes

$$\bar{P}(\mathbf{R}, \infty) = \int \rho(\mathbf{r}_0)\rho(\mathbf{r}_0 + \mathbf{R})\, d\mathbf{r}_0. \quad [89]$$

Thus, $\bar{P}(\mathbf{R}, \infty)$ is the autocorrelation function of the molecular density $\rho(\mathbf{r}_0)$ (or the convolution of the density with itself). From Eq. [87] and using the Wiener–Kintchine theorem (*82, 88*) (i.e., the Fourier transform of a time autocorrelation function is the frequency power spectrum), we find that $E(\mathbf{q}, \infty)$ is the power spectrum of $\rho(\mathbf{r}_0)$ (*41, 85, 89*),

$$\begin{aligned}
E(\mathbf{q}, \infty) &= \int \bar{P}(\mathbf{R}, \infty) e^{i2\pi\mathbf{q}\cdot\mathbf{R}}\, d\mathbf{R} \\
&= \iint \rho(\mathbf{r}_0)\rho(\mathbf{r}_0 + \mathbf{R})\, d\mathbf{r}_0 e^{i2\pi\mathbf{q}\cdot\mathbf{R}}\, d\mathbf{R} \\
&= \iint \rho(\mathbf{r}_0)\rho(\mathbf{r}_1)\, d\mathbf{r}_0 e^{i2\pi\mathbf{q}\cdot(\mathbf{r}_1 - \mathbf{r}_0)}\, d\mathbf{R} \\
&= \int \rho(\mathbf{r}_0) e^{-i2\pi\mathbf{q}\cdot\mathbf{r}_0}\, d\mathbf{r}_0 \int \rho(\mathbf{r}_1) e^{i2\pi\mathbf{q}\cdot\mathbf{r}_1}\, d\mathbf{r}_1 \\
&= S^*(\mathbf{q})S(\mathbf{q}) \\
&= |S(\mathbf{q})|^2 \quad [90]
\end{aligned}$$

where $S(\mathbf{q})$ is the Fourier transform of $\rho(\mathbf{r}_1)$. Alternately, Eq. [90] can easily be derived directly from Eqs. [75] and [88].

This is the origin of diffraction-like effects in PFG diffusion studies. In quasielastic neutron scattering $|S(\mathbf{q})|^2$ is known as the elastic incoherent structure factor, whereas in scattering theory it is referred to as the form factor of the confining volume (*86*). $S(\mathbf{q})$ is analogous to the signal measured in conventional NMR imaging (*41–43*). However, whereas conventional imaging returns the phase-sensitive spatial spectrum of the restricting pore, $E(\mathbf{q},\infty)$ measures the power spectrum, $|S(\mathbf{q})|^2$. Thus, $E(\mathbf{q},\infty)$ is sensitive to average features in local structure, not the motional characteristics. Further, because $E(\mathbf{q},\infty)$ measures the power spectrum of $S(\mathbf{q})$, Fourier inversion cannot be used to obtain a direct image of the pore. However, the **q**-space imaging has the potential to give much higher resolution than conventional **k**-space imaging, since the entire signal from the sample is available to contribute to each pixel in **R**-space (i.e., **R**, the dynamic displacement) (*85*) rather than from a volume element (i.e., voxel) as in conventional **k**-space imaging. Thus, the resolution achievable in **q**-space imaging is limited only by the magnitude of **q**.

We will illustrate the diffraction effect with recourse to diffusion in between parallel plates (see the inset to Fig. 6) with a separation of $2R$ (n.b. not **R**, the dynamic displacement). For this geometry, the analysis linking the experimental variables and the diffusion of the particle is performed in a manner entirely analogous to that already presented for free diffusion earlier, except that the mathematics is more tedious. Briefly, the solution to Eq. [26] for this geometry with the initial condition of Eq. [25] is given by (*66*)

$$P(z_0, z_1, t) = 1 + 2\sum_{n=1}^{\infty} \exp\left(-\frac{n^2\pi^2 Dt}{(2R)^2}\right) \times \cos\left(\frac{n\pi z_0}{2R}\right)\cos\left(\frac{n\pi z_1}{2R}\right). \quad [91]$$

If Eq. [91] is substituted into Eq. [75], except that we now write the equation in terms of q, we get the SGP solution (*56*),

$$E(q,\Delta) = \frac{2[1-\cos(2\pi q(2R))]}{(2\pi q(2R))^2} + 4(2\pi q(2R))^2 \sum_{n=1}^{\infty} \exp\left(-\frac{n^2\pi^2 D\Delta}{(2R)^2}\right) \times \frac{1-(-1)^n\cos(2\pi q(2R))}{\left[(2\pi q(2R))^2-(n\pi)^2\right]^2}. \quad [92]$$

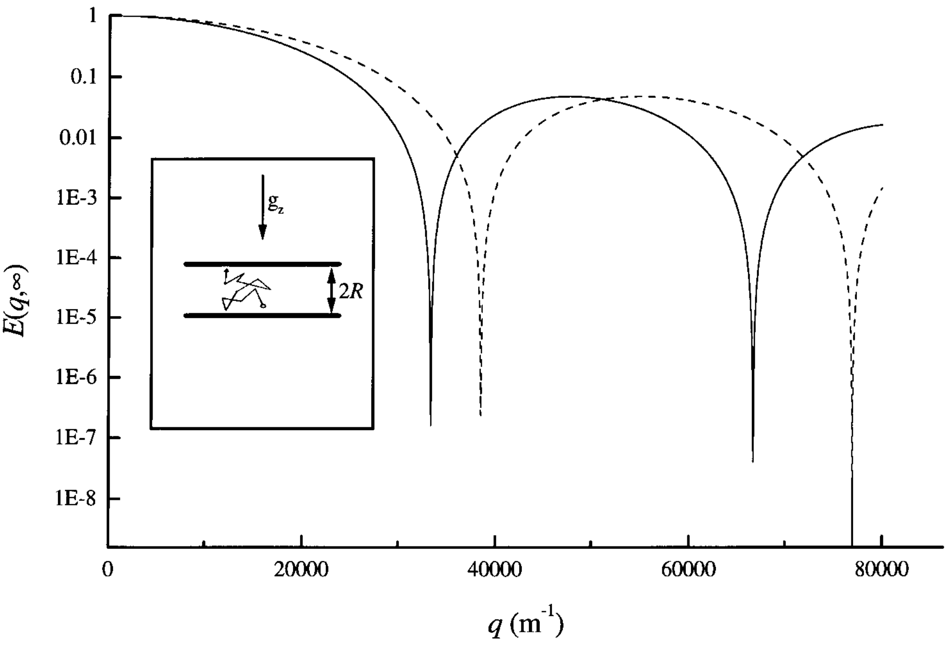

Figure 6 A plot of $E(q, \infty)$ versus q calculated using Eq. [93] for two values of the interplanar spacing (i.e., slit width; $2R$), $2R = 26$ μm (- - -) and 30 μm (——). The diffractive minima are clearly R dependent, and in the case of planes, the minima occur when $q = n/2R$ ($n = 1,2,3\ldots$). Generally, when there is only one characteristic distance, it is more convenient to plot the abscissa in terms of the dimensionless parameter qR (see Fig. 8).

In the long time limit $\xi \gg 1$ (i.e., $\Delta \to \infty$), Eq. [90] becomes

$$E(q, \infty) = \frac{2[1 - \cos(2\pi q(2R))]}{(2\pi q(2R))^2}$$
$$= |\mathrm{sinc}(\pi \mathrm{q}(2\mathrm{R}))|^2 \qquad [93]$$

where $\mathrm{sinc}(x) = \sin(x)/x$. $E(q, \infty)$ versus q is plotted for two values of R in Fig. 6. From Eq. [93], it is easy to see that diffractive minima result when $q = n/2R$ ($n = 1, 2, 3 \ldots$) and $E(\mathbf{q}, \infty) = 0$, since $\sin(n\pi) = 0$. The diffraction-like effects in the echo-attenuation curves clearly demonstrate that there is a direct analogy between the PFG diffusion measurement of a spin undergoing restricted diffusion in an enclosed pore and optical diffraction by a single slit (*89–92*). Also, the R-dependence of the attenuation curve also shows that structural information about the enclosing geometry can be obtained from the characteristics of the diffraction pattern. It is important to note that the above discussion regards diffusive (i.e., **q**-space) diffraction, not Mansfield (**k**-space) diffraction (*87, 93*). Mansfield (**k**-space) diffraction depends on the relative positions at fixed time [n.b., normal imaging returns an image of $\rho(\mathbf{r})$], whereas **q**-space diffraction depends on the relative displacements from the molecular origin during Δ.

The effects of diffraction and the experimental conditions that will lead to their observation are further considered in the following section.

PFG MEASUREMENTS IN RESTRICTED GEOMETRIES

General Relationships between $E(q, \Delta)$, q and Δ, and Displacement

The above discussion and considerations, especially Eqs. [85] and [88], reveal some pertinent points about the roles of Δ and $\mathbf{q}$ $(= (2\pi)^{-1}\gamma\delta\mathbf{g})$ in PFG diffusion measurements in systems in which the diffusion is restricted by barriers on a spatial scale of R. When the condition $qR \ll 1$ is met, the behavior of $E(\mathbf{q}, \Delta)$ is dominated by the diffusive motion of the spin. If the condition ξ $(= D\Delta/R^2) < 1$ is met, then the measured diffusion coefficient (i.e., D_{app}) will tend to that of the bulk solution (Fig. 4). As ξ increases, the effects of the restricting geometry will become increasingly important. When ξ is > 1, structural information can be obtained directly from the PFG signal (i.e., diffraction effects, if the restricting geometry has local order) by varying q such that $qR \geq 1$.

In analyzing the PFG dependencies for restricted geometries, one often implies an analogy to the free diffusion case and defines an apparent diffusion coefficient by

$$D_{app}(\Delta) = -\frac{1}{\Delta} \lim_{q \to 0} \frac{\partial \ln[E(q, \Delta)]}{\partial q^2}. \qquad [94]$$

The origin of Eq. [94] can be easily understood by substituting Eq. [82], written in terms of q for $E(q, \Delta)$. Considerable insight can be gained by performing a Taylor expansion (*51*) with $q = 0$ (i.e., Maclaurin's series) of Eq. [85] for the case of short Δ

$$E(\mathbf{q} \ll R^{-1}, \Delta)$$
$$\approx \int \bar{P}(\mathbf{R}, \Delta) \sum_{n=0}^{\infty} \frac{(i2\pi qR)^n}{n!} \frac{\partial^n e^{i2\pi \mathbf{q}\cdot\mathbf{R}}}{\partial \mathbf{q}^2}\, d\mathbf{R} \qquad [95]$$

For simplicity we assume that the gradient is directed along z (n.b. $Z = z_1 - z_0$), and thus from Eq. [95] we obtain (*14, 94, 95*),

$$E(\mathbf{q} \ll R^{-1}, \Delta)$$
$$\approx \int \bar{P}(Z, \Delta)\left[1 + \frac{i(2\pi q)Z}{1!} - \frac{(2\pi q)^2 Z^2}{2!}\right.$$
$$\left. - \frac{i(2\pi q)^3 Z^3}{3!} + \frac{(2\pi q)^4 Z^4}{4!} \cdots \right] dZ$$
$$= 1 - \frac{(2\pi q)^2 \langle z^2(\Delta)\rangle}{2!}$$
$$+ \frac{(2\pi q)^4 \langle z^4(\Delta)\rangle}{4!} \cdots \qquad [96]$$

In deriving the last step, we used Eq. [30]; also we note, by definition, that $\int_{-\infty}^{\infty} \bar{P}(Z, \Delta)\, dZ = 1$. As can be seen, all the odd orders vanish. From Eq. [96], we see that the initial decay of $E(\mathbf{q}, \Delta)$ with respect to q gives the mean-squared displacement

$\langle z^2(\Delta)\rangle$. Further, using Eq. [33], the apparent time-dependent diffusion coefficient can be obtained, i.e.,

$$D_{app}(\Delta) = \langle z^2(\Delta)\rangle \big/ (2\Delta) \qquad [97]$$

from the low q limit of $E(\mathbf{q}, \Delta)$. As might be expected, the time dependence of the apparent diffusion coefficient over observation time (i.e., Δ), such that Δ is finite but that $\langle z^2(\Delta)\rangle^{1/2}$ is less than the distance between the confinements, provides information on the surface-to-volume ratio of the confining geometry [see case (ii) in Fig. 4]. Mitra and coworkers (*96–98*) derived the relationship

$$D_{app}(\Delta) = D\left[1 - \frac{4}{3d\sqrt{\pi}}\frac{S_{geo}}{V}D^{1/2}\Delta^{1/2} + \cdots\right] \qquad [98]$$

where d is the number of spatial dimensions and S_{geo}/V is the surface-to-volume ratio. Thus, D_{app} deviates from D approximately linearly with $\Delta^{1/2}$. These surface effects have been nicely illustrated in a recent review by Callaghan and Coy (*14*).

The Validity of the Different Approaches

In the third section we presented three approaches for calculating the effects of diffusion on the signal attenuation in the PFG experiment. The macroscopic approach provides analytical solutions but is mathematically tractable only for free diffusion and for diffusion superimposed upon flow. We then presented the GPD and SGP approximations. It should be noted that these are not the only approximations available (e.g., Refs. (*99, 100*)]. In the case of free diffusion, the GPD approximation is valid and gives the same result as the macroscopic approach, while the SGP approximation gives the same result but in the limit of $\delta \to 0$ as $g \to \infty$. However, in chemical and biochemical systems (e.g., cells, micelles, zeolites, etc.), it is often the case that the diffusion of the probe species is restricted on the time scale of Δ (see Free and Restricted Diffusion), and to analyze the experimental data, the SGP or GPD approximation is normally used if the system is mathematically tractable. If the system is too complicated numerical methods must be resorted to.

It is important to understand the implications of the approximations involved in the GPD and SGP approaches [e.g., Refs. (*94, 101–104*)]. The validity of the GPD approach is determined by the validity of Eq. [57]. From the above discussion it was seen that the Gaussian phase approximation is justified in the case of free diffusion. Consequently, it will also hold in the case of restricted diffusion when Δ is so short that very few of the spins are affected by the boundary (i.e., $\xi \ll 1$; see earlier text and Fig. 2), since the propagator describing the restricted diffusion (i.e., $P(\mathbf{r}_0, \mathbf{r}_1, t)$) will reduce to that of the free diffusion case (i.e., Eq. [27]). Similarly, Neuman (*79*) showed that when Δ becomes so long that the probability of being at any position at the end of Δ is independent of the starting position, the change in phase becomes independent of the phase distribution. From the central limit theorem (*65*), the distribution of the sums of the phase changes becomes Gaussian. However, the enforcing of a Gaussian phase condition is a severe approximation and, as a consequence cannot yield interference effects (*105*).

In many experiments, particularly where the sample has a short T_2 relaxation time, which limits the value of Δ in the PFG pulse sequence, it may be impossible to comply closely enough with the requirements for SGP approximation. In this case, the GPD is useful, since it accounts for the finite length of the gradient pulse. However, the GPD approximation is exact only in the limit of free diffusion (i.e., $R \to \infty$); that is, where the phase distribution is Gaussian, while the SGP equation is only strictly valid for infinitely small δ. Balinov et al. (*101*) used computer simulations of Brownian motion to test the validity of the GPD and SGP approximations. They found that the GPD approximation solution for diffusion within a reflecting sphere (see Eq. [99] below) simulated the data very well in the limit of $\xi < 1$, fairly well for $\xi \approx 1$, and well for $\xi > 1$. In contrast, the SGP solution described the data well for large values of ξ and small gradient strengths. The results showed that at $\xi \approx 1$ the long time limit of the SGP equation (i.e., the attenuation has become independent of Δ) is already applicable (*101*). Blees (*102*) and others [e.g., (*94, 105*)], using numerical simulations, considered the effects of finite δ on the SGP approximation solution (Eq. [92]) for spin diffusing between reflecting planes (Fig. 6). They found that as the duration of the gradient pulse becomes finite, the diffraction minima shift toward higher q. The higher-order minima were more affected than the first minimum.

In the next section, we will illustrate some aspects of the above discussion by comparing the results for a diffusion inside a sphere obtained using the GPD and SGP approximations. In the present case, we consider the (relatively) simple case of spins within a reflecting sphere (i.e., the sphere is impermeable and collision with the surface of the sphere does not affect the relaxation of the spins).

An Example: Diffusion Within a Sphere

Although mathematical models have been derived for a number of complicated geometries for both steady and PFG sequences [e.g., (*12, 79, 105–111*)], here we will consider only the theoretical solutions for the PFG experiment obtained using the SGP and GPD approximations for diffusion within reflecting spherical boundaries of radius R. A reflecting sphere is a suitable first approximation for the diffusion of small molecules such as metabolites inside cells (*71*), or molecules inside many porous systems. In agreement with the earlier discussion concerning free and restricted diffusion, the solutions for the restricting geometries reduce to those for free diffusion in the short time limit (i.e., $\xi < 1$), while in the long time limit (i.e., $\xi > 1$) the solutions become dependent upon only the restricting geometry.

The GPD approximation solution for a spin diffusing within a reflecting sphere is calculated analogously to the case of free diffusion as given previously. The solution is given by (*106*)

$$E(q,\Delta) = \exp\left(-\frac{2\gamma^2 g^2}{D^2} \times \sum_{n=1}^{\infty} \frac{2\alpha_n^2 D\delta - 2 + 2L(\delta) - L(\Delta-\delta) + 2L(\Delta) - L(\Delta+\delta)}{\alpha_n^6 (R^2\alpha_n^2 - 2)} \right) \qquad [99]$$

where $L(t) = \exp(-\alpha_n^2 D t)$ and α_n are the roots of the equation

$$(\alpha_n R) J'_{3/2}(\alpha_n R) - 1/2 J_{3/2}(\alpha_n R) = 0,$$

where J is the Bessel function of the first kind [e.g., Ref. (*52*)]. Similarly, the SGP solution is calculated in the same manner as the free-diffusion example given previously. The solution is (*101*)

$$\begin{aligned} E(q,\Delta) = {} & \frac{9[(2\pi qR)\cos(2\pi qR) - \sin(2\pi qR)]^2}{(2\pi qR)^6} \\ & + 6(2\pi qR)^2 \sum_{n=0}^{\infty} [j'_n(2\pi qR)]^2 \\ & \times \sum_m \frac{(2n+1)\alpha_{nm}^2}{\alpha_{nm}^2 - n^2 - n} \\ & \times \exp\left(-\frac{\alpha_{nm}^2 D\Delta}{R^2} \right) \frac{1}{\left[\alpha_{nm}^2 - (2\pi qR)^2\right]^2} \end{aligned} \qquad [100]$$

where α_{nm} is the mth nonzero root of the equation $j'_n(\alpha_{nm}) = 0$ and j is the spherical Bessel function of the first kind [e.g., Ref. (*52*)].

As an example of the effects of restricted diffusion, we have plotted some simulated data for free diffusion and diffusion within a sphere (using the GPD approximation) in Fig. 7 using the same experimental conditions and gradient strength as in Fig. 5. To show the effects clearly we have chosen to plot the data as a function of Δ. As is readily apparent in the case of free diffusion, the mean-squared displacement scales with time, and as a result we obtain a straight line. However, in the case of diffusion within a sphere, at very small values of Δ the results of the simulation agree with that for free diffusion, but as Δ increases, there is a transition from free diffusion to surface effects as the boundaries significantly affect the motion of the diffusing spins, and the mean-squared displacement no longer scales linearly with time (i.e., the diffusion is no longer purely Gaussian). At large values of Δ, the motion becomes completely restricted, the displacement becomes time independent, and the attenuation curve plateaus out.

It is very interesting to compare the long-time (i.e., $\xi \to \infty$) behavior of Eqs. [99] and [100]. In Eq. [99], all the $L(t)$ terms involving Δ disappear, leaving only an exponential function involving δ and D; thus, Eq. [99] becomes (*79*)

$$E(q,\infty) = \exp\left(-(2\pi qR)^2/5\right), \qquad [101]$$

a monotonically decreasing function. However, in the cases of Eq. [100], we have a totally different situation, as only the second term on the right-hand side of Eq. [100] vanishes [n.b., the

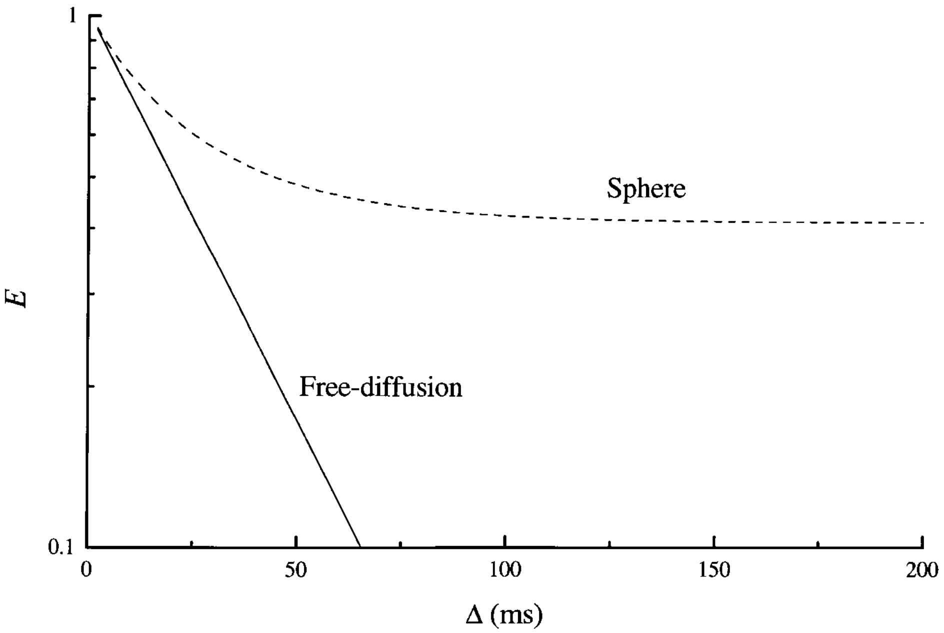

Figure 7 A plot of simulated echo attenuation in the case of free diffusion (——) and diffusion in a sphere (– – –) based on the GPD approximation (i.e., Eq. [99]) versus Δ. The parameters used in the simulation were $\delta = 1$ ms, $D = 5 \times 10^{-10}$ m^{2}s^{-1}, $g = 1$ T m^{-1}, $R = 8$ μm, and $\gamma = \gamma^{^1\mathrm{H}} = 2.6571 \times 10^8$ rad T^{-1}s^{-1}. The echo attenuation in the case of diffusion in the sphere can be seen to go through three stages: (i) when $\xi \ll 1$, the diffusion appears unrestricted and the result is the same as that of free diffusion, (ii) as Δ increases the spins begin to feel the effects of the surface, and (iii) when $\xi > 1$, the diffusion is fully restricted and the attenuation curve plateaus out.

$\exp(-\alpha_{nm}^2\xi)$ term] leaving the trigonometric (i.e., periodic) function

$$E(q,\infty) = \frac{9[(2\pi qR)\cos(2\pi qR) - \sin(2\pi qR)]^2}{(2\pi qR)^6}. \tag{102}$$

Obviously, as q increases, the denominator of Eq. [102] increases (such that Eq. [102] as a whole decreases), but the trigonometric functions in the numerator result in the function having an infinite series of maxima and minima. The minima occur when q takes a value such that $(2\pi qR)\cos(2\pi qR) - \sin(2\pi qR) = 0$, for the first minima, this occurs when $q \approx 0.71/R$. The simulated echo intensity calculated using both the GPD and SGP approximations versus qR is shown in Fig. 8. We can see that at small attenuation values, the GPD and SGP approximations agree very well (n.b., $\delta \ll \Delta$), but at larger attenuation values, the SGP approximation gives diffractive minima, whereas as expected, the GPD approximation does not. In well-chosen systems where the signal-to-noise ratio is sufficient and the sample geometry is monodisperse (or at least not too polydisperse), it is possible to observe such minima [e.g., (*105*)]. The diffractive minima are an additional source of information and their position is R dependent.

Anisotropic Diffusion

Earlier, it was noted that isotropic diffusion is really just a special case, and more generally, we must consider anisotropic diffusion resulting from either the physical arrangement of the medium or anisotropic (i.e., nonspherical) restriction. Such situations commonly arise in biological (e.g., cells, skeletal muscle) and liquid crystals systems [e.g., Refs. (*112, 113*) and references therein], thus the diffusion process is represented by a Cartesian tensor, **D** (see Free and Restricted Diffusion). In such systems, the echo-signal attenuation will have an orientational dependence with respect to the measuring gradient. For example, for anisotropic free diffusion, the g^2D term in Eq. [51] must be replaced by $\mathbf{g} \cdot \mathbf{D} \cdot \mathbf{g}$, where

$$\mathbf{g} \cdot \mathbf{D} \cdot \mathbf{g} = \sum_{\alpha} \sum_{\beta} D_{\alpha\beta} g_\alpha g_\beta \quad \alpha, \beta = x, y, z \tag{103}$$

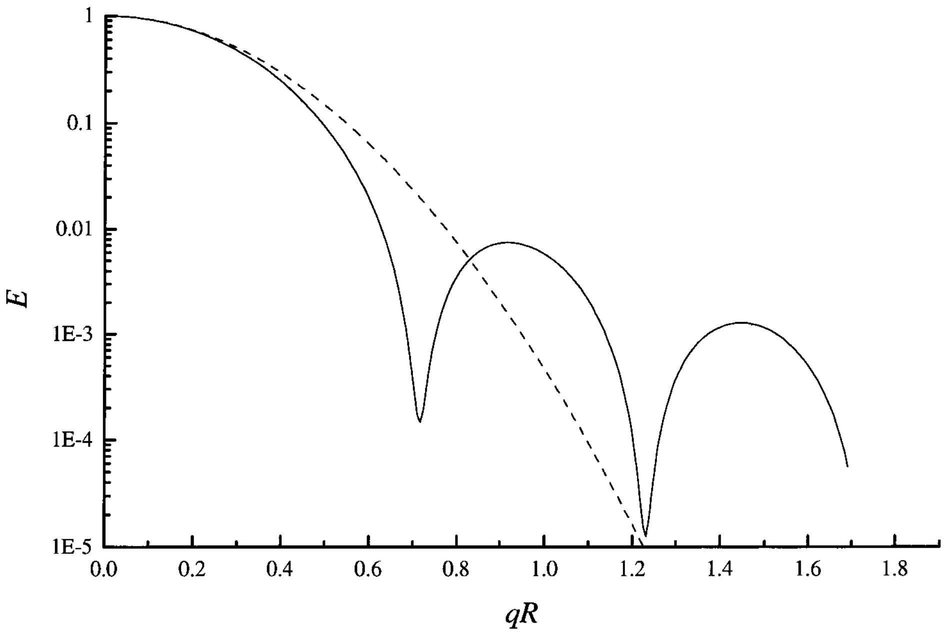

Figure 8 A plot of the simulated echo-attenuation data for diffusion within a sphere calculated using the SGP approximation (——) and the GPD approximation (– – –) versus qR. The parameters used in the simulation were $\delta = 1$ ms, $\Delta = 100$ ms, $D = 1 \times 10^{-9}$ m^{2}s^{-1}, $g = 1$ T m^{-1}, $R = 8$ μm, and $\gamma = \gamma^{^1\mathrm{H}} = 2.6571 \times 10^8$ rad T^{-1}s^{-1}. The minima in the SGP plot occur when q takes a value such that the numerator in Eq. [102] equates to 0.

and so we obtain (*55*)

$$\ln(E) = -\gamma^2 \mathbf{g}\cdot\mathbf{D}\cdot\mathbf{g}\delta^2(\Delta - \delta/3). \qquad [104]$$

We remark that Eq. [104] can be rewritten in a form similar to Eq. [53], i.e.,

$$\ln(E) = -\sum_{\alpha}\sum_{\beta} b_{\alpha\beta}D_{\alpha\beta} = -\mathbf{b}{:}\mathbf{D} \qquad [105]$$

where ":" is the generalized dot product and **b** is now a symmetric matrix given by (*114*)

$$\begin{aligned}\mathbf{b} &= \gamma^2\int_0^{2\tau}(\mathbf{F}(t') - 2H(t-\tau)\mathbf{f})\\ &\quad\times(\mathbf{F}(t') - 2H(t-\tau)\mathbf{f})^T\,dt\\ &= \gamma^2 g_\alpha g_\beta \delta^2(\Delta - \delta/3). \qquad [106]\end{aligned}$$

The first line in Eq. [106] is a general definition and the second line is the specific solution for the PFG sequence. Alternatively and totally equivalently, we can rewrite Eq. [52] as

$$\ln(E(t)) = -\gamma^2\int_0^t \mathbf{F}\cdot\mathbf{D}\cdot\mathbf{F}\,dt. \qquad [107]$$

From Eq. [104], it can be seen that the direction in which the diffusion is measured is determined by the gradient, and it is actually a diagonal element of **D**, the diffusion tensor in the gradient frame, that is measured. Thus, the equation relating the echo attenuation due to free diffusion when measured using a z-gradient (i.e., Eq. [51]) written in tensor notation is

$$\ln(E) = -\gamma^2 g_z^2 D_{zz}\delta^2(\Delta - \delta/3) = -b_{zz}D_{zz}. \qquad [108]$$

The diffusion tensor in the molecular frame, **D**′, can be transformed to the laboratory (i.e., gradient frame) (Fig. 9) by using rotation matrices [e.g., Ref. (*115*)]

$$\mathbf{D} \equiv \mathbf{R}^{-1}(\theta,\varphi)\cdot\mathbf{D}'\cdot\mathbf{R}(\theta,\varphi) \qquad [109]$$

where $\mathbf{R}(\theta,\varphi)$ is the relevant rotation matrix and θ and φ are the polar and azimuthal angles between the director and gradient frames, respectively. Thus, the off-diagonal elements of **D** will vanish only when the director and laboratory frames of reference coincide. Thus, in the general case, both diagonal and off-diagonal elements of

D′ will affect the measured echo attenuation (*114, 116*).

The situation with anisotropic restricted diffusion is more complicated, and we will illustrate this with reference to diffusion in a cylinder with an arbitrary (polar) angle, θ, between the symmetry axis of the cylinder and the static magnetic field (which is also the direction of the gradient) (Fig. 9). Such a cylinder can be thought of, for example, as a simplistic model of a muscle-fiber cell. The SGP solution for this geometry is given by (*117*)

$$E(q,\Delta) = \sum_{n=0}^{\infty}\sum_{k=1}^{\infty}\sum_{m=0}^{\infty} \frac{2K_{nm}R^2(2\pi qR)^4\sin^2(2\theta)\left[1-(-1)^n\cos(2\pi qL\cos\theta)\right]\alpha_{km}^2}{L^2\left[(n\pi R/L)^2-(2\pi qR)^2\cos^2\theta\right]^2\left[\alpha_{km}^2-(2\pi qR)^2\sin^2\theta\right]^2(\alpha_{km}^2-m^2)} \times[J'_m(2\pi qR\sin\theta)]^2\exp\left\{-\left[\left(\frac{\alpha_{km}}{R}\right)^2+\left(\frac{n\pi}{L}\right)^2\right]D\Delta\right\} \qquad [110]$$

where L is the length of the cylinder, R is the radius of the cylinder, and α_{km} is the kth nonzero root of the equation $J'_m(\alpha_{km}) = 0$, where J is the Bessel function of the first kind, and the constant K_{nm} depends on the values of the indexes n and m according to

$$\begin{aligned} K_{nm} &= 1 \quad \text{if } n = m = 0\\ K_{nm} &= 1 \quad \text{if } n \neq m = 0 \text{ or } m \neq 0 \text{ and } n = 0\\ K_{nm} &= 1 \quad \text{if } n, m \neq 0. \end{aligned} \qquad [111]$$

Now, the mathematical complexity is no concern to us here and the point that we wish to emphasize is the θ dependence; thus, in contradistinction to the cases of free diffusion and diffusion with a sphere, in an anisotropic system the spin-echo attenuation is now a function of the direction of the gradient. In fact, if we had a less symmetric geometry (e.g., an elliptic cylinder), then the equation for $E(q,\Delta)$ should also be dependent on the azimuthal angle, φ. If we set $\theta = 0$, then the solution given by Eq. [110] reduces, as expected, to the solution for diffusion between planes (i.e., Eq. [92] and noting that $L = 2R$). Similarly, if $\theta = \pi/2$, Eq. [110] reduces to the solution for diffusion in a cylinder (*110*),

$$E(q,\Delta) = 2(2\pi qR)^2\sum_{k=1}^{\infty}\sum_{m=0}^{\infty}\frac{K_{0m}\alpha_{km}^2[J'_m(2\pi qR)]^2\exp\left\{-(\alpha_{km}/R)^2D\Delta\right\}}{\left[\alpha_{km}^2-(2\pi qR)^2\right]^2(\alpha_{km}^2-m^2)}. \qquad [112]$$

The echo-attenuation curves for diffusion in a cylinder versus Δ are plotted for three different values of θ in Fig. 10. The long time limiting formula for the cylinder is given by (*117*)

$$E(q,\infty) = \frac{8R^2[1-\cos(2\pi qL\cos\theta)][J_1(2\pi qR\sin\theta)]^2}{(2\pi qR)^4L^2(\cos\theta\sin\theta)^2}. \qquad [113]$$

When $\theta = 0$, this, of course, reduces to the long time for diffusion between planes as given in Eq. [93] (n.b. $L = 2R$), and when $\theta = \pi/2$, this reduces to (*117*)

$$E(q,\infty) = \frac{[2J_1(2\pi qR)]^2}{(2\pi qR)^2}. \qquad [114]$$

The echo-attenuation curves for diffusion in a cylinder versus qR are plotted for three different values of θ in Fig. 11.

Clearly, the θ dependence on the attenuation curves and the diffraction patterns—or alternately, we can think of this as the orientation of **D** with respect to the gradient—provides an additional structural probe. If the restricted diffusion effects are not accounted for and free diffusion is assumed, and Eq. [104], which is valid only for free diffusion, is used to analyze the attenuation data, then **D**′ is really an apparent diffusion tensor, $\mathbf{D}'_{app}$. When a single effective diffusion tensor is estimated for the entire sample, it is sometimes referred to as "diffusion tensor MR spectroscopy," and when, as is commonly the case in imaging studies, the estimation is performed for each voxel, it is referred to as "diffusion tensor MR imaging." From the discussion on restricted diffusion above it should be clear that $\mathbf{D}'_{app}$ is perhaps better written as $\mathbf{D}'_{app}(\Delta)$, since it will be observation time dependent. For sufficiently short values of Δ such that the diffusion of the probe species is unaffected by the boundaries, $\mathbf{D}'_{app}(\Delta)$ would be isotropic, whereas for larger Δ, it becomes increasingly anisotropic. This can be easily visualized from the divergence of the echo-signal attenuation plots for different values of θ versus Δ given in Fig. 10. For the case of diffusion within a cylinder (Fig. 9), $\mathbf{D}'_{app}$ would be given by

$$\mathbf{D}'_{app} = \begin{bmatrix} D'_{xx} & 0 & 0 \\ 0 & D'_{yy} & 0 \\ 0 & 0 & D'_{zz} \end{bmatrix} \qquad [115]$$

where $D'_{xx} = D'_{yy}$ owing to the axial symmetry of the cylinder. We remark that D'_{xx}, D'_{yy}, and D'_{zz} are, of course, eigenvalues of the matrix $\mathbf{D}'_{app}$ and are often termed the "principal diffusivities." Ideally, it is possible to determine the dimensions of the restricting geometry from the restricted displacement—for example, in the case of the cylinder, the long axis of the cylinder gives the largest apparent diffusion coefficient—but this requires prior knowledge of the sample orientation so that it is possible to align the director frame of reference coincident with the gradient frame of reference in the PFG experiment. Sometimes it is useful to represent $\mathbf{D}'_{app}$ graphically by a diffusion ellipsoid (45) (Fig. 12), which can be constructed using

$$\left(\frac{x'}{\sqrt{2D'_{xx}\Delta}}\right)^2 + \left(\frac{y'}{\sqrt{2D'_{yy}\Delta}}\right)^2 + \left(\frac{z'}{\sqrt{2D'_{zz}\Delta}}\right)^2 = 1. \qquad [116]$$

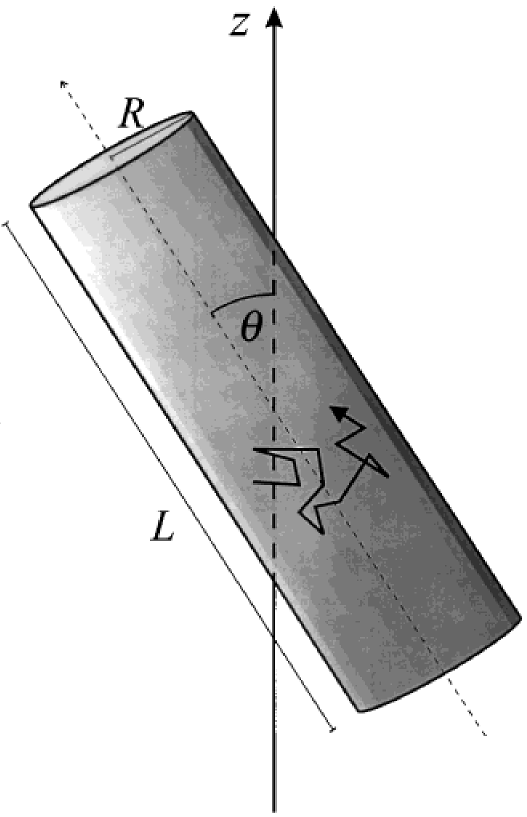

Figure 9 Schematic diagram of diffusion in a cylinder. The cylinder is of length L and radius R with the symmetry axis of the cylinder (– – –) subtends an angle θ with the direction of the gradient and static field, which is taken to be z in the present case. The laboratory or gradient frame is given by (x, y, z), where z coincides with the gradient direction. The director frame for the cylinder is given by (x', x', z'), where z' coincides with the symmetry axis of the cylinder. If this were an elliptic cylinder for example, the director frame would be uniquely determined. Clearly, if $\theta = 0$, the two reference frames coincide. If $\theta = 0$ and a PFG diffusion measurement is performed, the spin-echo attenuation will be described by diffusion between planar boundaries (i.e., Eq. [92]). Conversely, if $\theta = \pi/2$, the spin-echo attenuation will be described by diffusion within a cylinder (Eq. [112]).

Equation [116] can be derived starting from Eq. [27], but substituting the $\mathbf{D}'_{app}$ for the scalar D. We note from Eq. [33] that the major axes of the ellipsoids in Eq. [116] are the mean diffusion distances (i.e., $\sqrt{\langle x'^2 \rangle} = \sqrt{2D_{xx}\Delta}$, etc.). As $\mathbf{D}'_{app}$ becomes more anisotropic the ellipsoid becomes more prolate. For example, in muscle fiber, the effective diffusion ellipsoid reflects the fiber orientation and the mean diffusion distances.

Generally, the relative alignment between the gradient and director frames is not known, the diffusion measurement returns a mixture of the different elements of the diffusion tensor, and the orientational dependence becomes a problem.

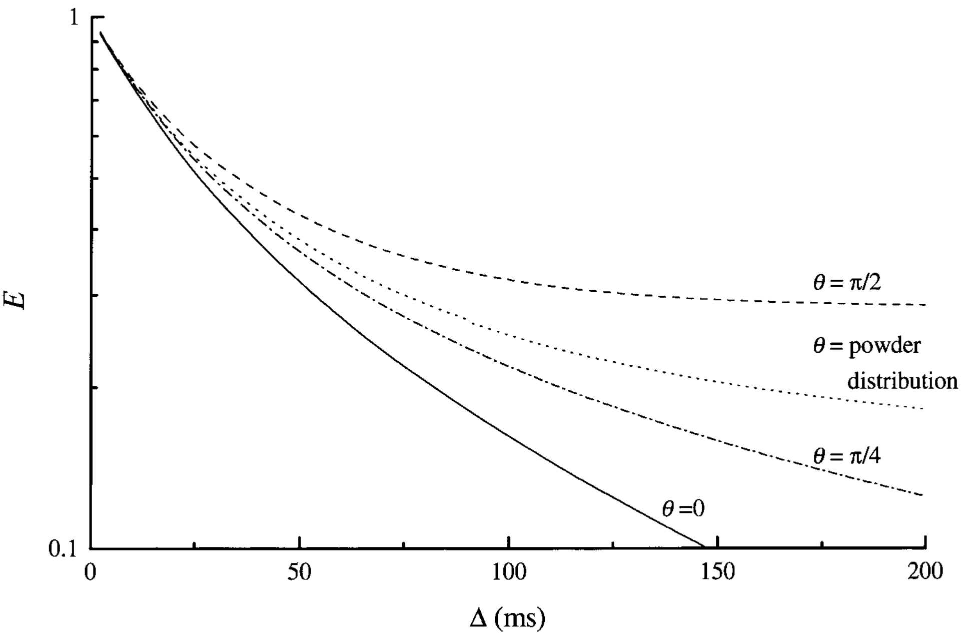

Figure 10 A plot of the simulated echo attenuation for PFG diffusion measurements in a cylinder with the cylinder oriented at three different polar angles with respect to the gradient, i.e., $\theta = 0$ (——), $\theta = \pi/4$ (–·–·–), and $\theta = \pi/2$ (– – – –) versus Δ calculated using Eqs. [92], [110], and [112], respectively. Also shown is the result of a power distribution of polar angles (······) versus Δ calculated using Eqs. [110] and [119]. The parameters used in the simulation were the same, as far as possible, as those used for the sphere in Fig. 7, i.e., $\delta = 1$ ms, $D = 5 \times 10^{-10}$ m^{2}s^{-1}, $g = 1$ T m^{-1}, $R = 8$ μm, $L = 24$ μm, and $\gamma = \gamma^{^1\mathrm{H}} = 2.6571 \times 10^8$ rad T^{-1}s^{-1}. The effects of the polar angle can be clearly seen on the attenuation curves, and the curves go through three stages depending on Δ (this is most obvious in the $\theta = \pi/2$ case), similar to the results for diffusion in a sphere (see Fig. 7). As would be expected, since it is an average over all possible polar angles, the powder average echo-attenuation curve is between the limits of the attenuation curves for $\theta = 0$ and $\theta = \pi/2$. Because of the axial symmetry of the cylinder, it was unnecessary to average over φ. However, the normalization factor in Eq. [119] was changed appropriately.

For example, it makes it difficult to compare the diffusional characteristics of one sample to another. A solution is to determine **D**′ itself by measuring the diffusion coefficients in seven different directions [i.e., except for the case of charged moieties, **D**′ is symmetric (*118*) and so there are only six independent elements]. However, because of experimental imprecision it is normal to perform a much larger number of measurements and determine **D**′ statistically (*114*). As seen in Eq. [108], the use of a single gradient direction in a diffusion measurement allows the diagonal elements of **D** to be probed. The off-diagonal elements can be probed by applying gradients along various oblique directions (consider the pulse sequence shown in Fig. 2, but with the possibility of gradients along all three Cartesian directions). For example, if gradients were applied along all three Cartesian directions, then the echo attenuation would be described by (i.e., Eq. [105])

$$\begin{aligned}\ln(E) = -\big[&b_{xx}D_{xx} + b_{yy}D_{yy} + b_{zz}D_{zz}\\ &+(b_{xy} + b_{yx})D_{xy} + (b_{xz} + b_{zx})D_{xz}\\ &+(b_{yz} + b_{zy})D_{yz}\big]. \qquad [117]\end{aligned}$$

As a further complication, the restricting geometries may not all be uniformly aligned in the same direction [e.g., brain white matter (*119*)] or even randomly aligned (e.g., a suspension of red blood cells). The apparent **D**′ is then an average of the different orientations. Measuring diffusion in three orthogonal directions so as to determine the trace of the diffusion tensor has been pro-

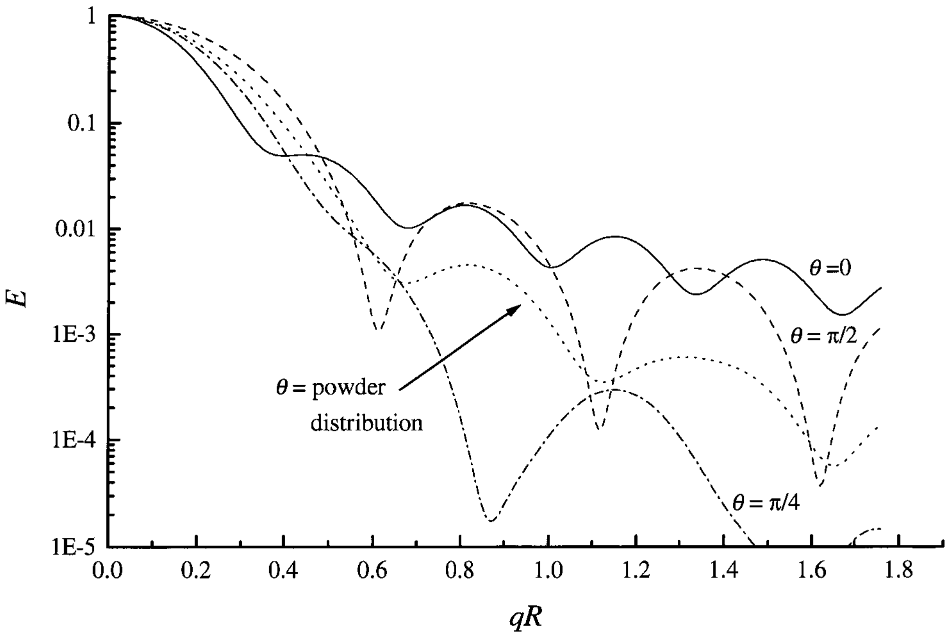

Figure 11 Plot of the simulated echo attenuation for PFG diffusion in a cylinder with the cylinder oriented at three different polar angles with respect to the gradient, i.e., $\theta = 0$ (——), $\theta = \pi/4$ (–·–·–), and $\theta = \pi/2$ (– – –) versus qR calculated using Eq. [92], [110], and [112], respectively. Also shown is the result of a powder distribution of polar angles (······) versus qR calculated using Eqs. [110] and [119]. The parameters used in the simulation were the same, as far as possible, as those used for the sphere in Fig. 8, i.e., $\delta = 1$ ms, $D = 1 \times 10^{-9}$ m^{2}s^{-1}, $g = 1$ T m^{-1}, $R = 8$ μm, $L = 24$ μm, and $\gamma = \gamma^{^1\mathrm{H}} = 2.6571 \times 10^8$ rad T^{-1}s^{-1}. The effects of the polar angle can be clearly seen on the attenuation curves and the position of the diffraction minima. The behavior of the diffractive minima is quite different from that found for the sphere in Fig. 8.

posed as a means of overcoming the anisotropy problems (*45, 120*)

$$\frac{1}{3}\mathrm{Tr}(\mathbf{D}') = \frac{1}{3}(D'_{xx} + D'_{yy} + D'_{zz}) = \frac{1}{3}\mathrm{Tr}(\mathbf{D}) = \frac{1}{3}(D_{xx} + D_{yy} + D_{zz}) = D_{av}. \quad [118]$$

As the trace is invariant under rotations, the orientational dependence is removed (i.e., from Eq. [118], the trace of the diffusion tensor in the director or cell frame equals the trace of the diffusion tensor in the gradient frame). For completion, we should note that where the diffusion tensor is observation time dependent, as it is in the case of restricted diffusion, and under some experimental circumstances, the measured trace can differ from the true trace of the effective diffusion tensor and the measured quantity is not completely rotationally invariant (*121*).

Generally, however, diffusion is only measured in one direction, and if the anisotropic system is not oriented in one direction, it is necessary to perform a powder average. In performing the powder average, it is mathematically equivalent to consider that there is only a single domain with a defined direction and that it is the field gradient randomly oriented (*122*); thus,

$$E(\mathbf{g}, \Delta)_{powder} = \frac{1}{4\pi}\int_0^{2\pi}\int_0^{\pi} E(\mathbf{g}, \Delta, \theta, \varphi)\sin\theta \, d\theta \, d\varphi \quad [119]$$

where $(1/4\pi)\sin\theta\, d\theta\, d\varphi$ is the probability of $\mathbf{g}$ being in the direction defined by θ and φ, and we have written $E(\mathbf{g}, \Delta, \theta, \varphi)$ to emphasize the orientational dependence of the attenuation. The powder average of the echo attenuation due to diffusion in a cylinder (i.e., Eq. [110]) is plotted against Δ and qR in Figs. 10 and 11, respectively. The situation is much more complicated, though, if in the time scale of Δ the diffusing molecules change from one domain (e.g., exchange between cells), specified by a unique local director orientation, into another (*123, 124*). Exact solutions to Eq. [119] are known only for some very simple cases [e.g., Refs. (*41, 124, 125*)] and generally, Eq. [119] must be evaluated numerically (*122, 124*).

CONCLUDING REMARKS

Pulsed-field gradient experiments provide a straightforward means of obtaining information on the translational motion of nuclear spins. However, the interpretation of the data is complicated by the effects of restricting geometries and the mathematical modeling required to account for this becomes nontrivial for anything but the simplest of geometries. Generally, we have to resort to numerical methods and/or approximations to model diffusion within restricted geometries, and the type of approximation that we choose should be consistent with our experimental conditions. For example, to use the SGP approximation we must ensure that the condition $\delta \ll \Delta$ holds.

In the present article we have presented the underlying concepts of how PFGs may be used to measure diffusion. The mathematical modeling required to extract information from the attenuation of the echo signal on the diffusion process and structural information in restricting geometries was presented in some detail, and both isotropic and anisotropic systems were considered. However, the experimental aspects and complications were largely ignored. Further, we presented only simple examples of restricting geometries and have barely mentioned any of the many applications that PFG NMR can be applied to such as measuring polymer dynamics, obtaining diffusion and structural information in porous media with more complicated restricted geometries and measuring exchange.

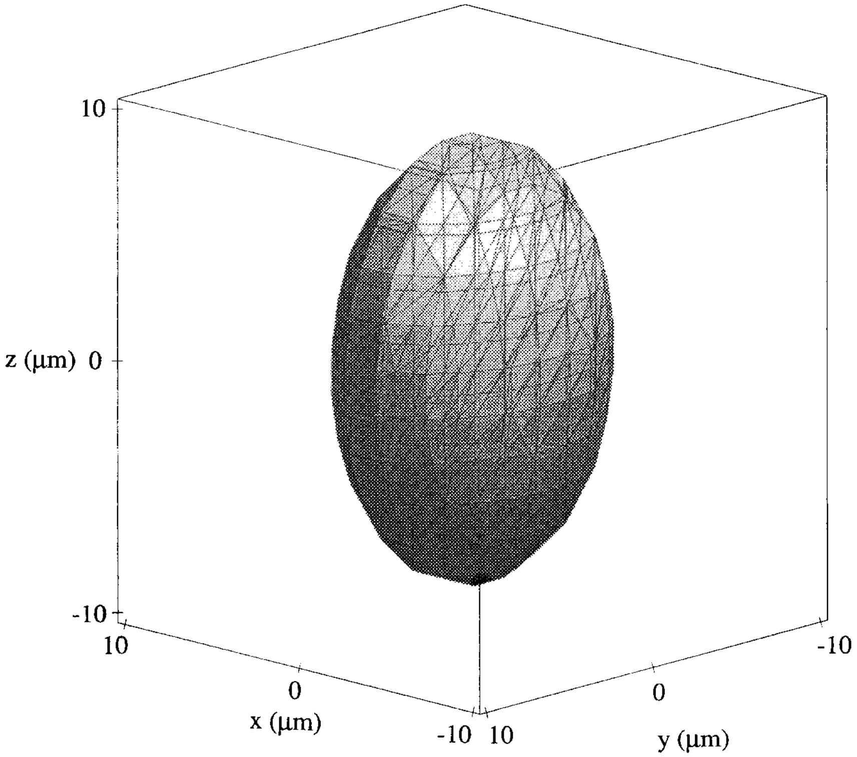

Figure 12 Example of an effective diffusion ellipsoid calculated using Eq. [116]. The parameters used in the simulation were Δ = 20 ms, $D_{xx} = 0.6 \times 10^{-9}$ m^{2}s^{-1}, $D_{yy} = 1.2 \times 10^{-9}$ m^{2}s^{-1}, $D_{zz} = 1.5 \times 10^{-9}$ m^{2}s^{-1}. The extremely anisotropic diffusion parameters were chosen to allow easy visualization of the ellipsoidal shape.

Experimental aspects of PFG NMR will be presented in Part II of the series.

APPENDIX

Maple Worksheet for the Stejskal and Tanner Equation

Define the integral used in determining F

```
> F:= (g, ti) → int (g, td = ti..t);
```

$$F := (g, ti) \rightarrow \int_{ti}^{t} g\, dtd$$

Define the time intervals and the relevant value of g for each integral. Also calculate the value of F for each interval remembering that it contains the contribution from all of the intervals from the start of the pulse sequence.

```
> l1:= 0;
> g1:= 0;
> F1:= F(g1, 11);
```

$$l1 := 0$$
$$g1 := 0$$
$$F1 := 0$$

```
> l2:= t1;
> g2:= g;
> F2:= subs(t = l2, F1) + F(g2, l2);
```

$$l2 := t1$$
$$g2 := g$$
$$F2 := tg - t1g$$

```
> l3:= t1 + delta;
> g3:= 0;
> F3:= subs(t = l3, F2) + F(g3, l3);
```

$$l3 := t1 + \delta$$
$$g3 := 0$$
$$F3 := (t1 + \delta)g - t1g$$

```
> l4:= t1 + Delta;
> g4:= g;
> F4:= subs(t = l4, F3) + F(g4, l4);
```

$$l4 := t1 + \Delta$$
$$g4 := g$$
$$F4 := (t1 + \delta)g - 2t1g + tg - g\Delta$$

```
> l5:= t1 + Delta + delta;
> g5:= 0;
> F5:= subs(t = l5, F4) + F(g5, l5);
> l6:= 2* tau;
```

$$l5 := t1 + \Delta + \delta$$
$$g5 := 0$$
$$F5 := (t1 + \delta)g - 2t1g + (tl + \Delta + \delta)g - g\Delta$$
$$l6 := 2\tau$$

Define the function "f" [= F(tau)]

```
> f:= subs(t = tau, F3);
```

$$f := (t1 + \delta)g - t1g$$

Define the integral of F between tau and 2* tau

```
> FINT:= int(F3, t = tau..l4) + int(F4, t = l4..l5)
+int(F5, t = l5..l6);
```

$$FINT := -g\delta t1 - g\delta\Delta + 3\tau g\delta - \tfrac{1}{2}g\delta^2$$

Define the integral of F ^2 between 0 and 2* tau

```
> FSQINT := int(F1^2, t = l1..l2)
  +int(F2^2, t = l2..l3)
  +int(F3^2, t = l3..l4)
  +int(F4^2, t = l4..l5) + int(F5^2, t = l5..l6);
```

$$FSQINT := -\tfrac{7}{3}g^2\delta^3 - 3g^2\delta^2\Delta + 8\tau g^2\delta^2 - 4g^2\delta^2\, t1$$

Define the function to give the Stejskal and Tanner relationship and simplify the result.

```
> ln(E) := simplify(-gamma^2*D*(FSQINT -
  4*f*FINT + 4*f^2*tau));
```

$$\ln(E) := \tfrac{1}{3}\gamma^2 D g^2\delta^2(\delta - 3\Delta)$$

ACKNOWLEDGMENT

Dr. A. V. Barzykin, Dr. K. Hayamizu, and Dr. P. van Gelderen are thanked for critically reading the manuscript and their valuable suggestions. The author is also very grateful for the very detailed comments provided by the referees.

REFERENCES

1. E. Hawlicka, "Self-Diffusion in Multicomponent Liquid Systems," *Chem. Soc. Rev.*, **1995**, *34*, 13743–13750.
2. R. J. Hunter, *Foundations of Colloid Science*, Oxford University Press, Oxford, 1986.
3. M. A. Lauffer, *Motion in Biological Systems*, Alan R. Liss, New York, 1989.
4. A. G. Marshall, *Biophysical Chemistry Principles, Techniques, and Applications*, Wiley, New York, 1978.
5. D. C. Teller, E. Swanson, and C. De Haën, "The Translational Friction Coefficient of Proteins," *Methods Enzymol.* **1979**, *61*, 103–124.
6. J. G. de la Torre and V. Bloomfield, "Hydrodynamic Properties of Complex, Rigid, Biomolecules: Theory and Applications," *Q. Rev. Biophys.*, **1981**, *14*, 81–139.
7. J. G. de la Torre, S. Navarro, M. C. L. Martinez, F. G. Diaz, and J. J. L. Cascales, "HYDRO: A Computer Program for the Prediction of Hydrodynamic Properties of Macromolecules," *Biophys. J.* **1994**, *67*, 530–531.
8. D. E. Woessner, "Brownian Motion and Correlation Times," in *Encyclopedia of Nuclear Magnetic Resonance*, D. M. Grant and R. K. Harris, Eds. Wiley, New York, 1996, pp. 1068–1084.
9. D. E. Woessner, "Relaxation Effects of Chemical Exchange," in *Encyclopedia of Nuclear Magnetic Resonance*, D. M. Grant and R. K. Harris, Eds. Wiley, New York, 1996, pp. 4018–4028.
10. R. Lenk, *Fluctuations, Diffusion and Spin Relaxation*, Elsevier, Amsterdam, 1986.
11. P. Stilbs, "Fourier Transform Pulsed-Gradient Spin-Echo Studies of Molecular Diffusion," *Progr. NMR Spectrosc.* **1987**, *19*, 1–45.
12. J. Kärger, H. Pfeifer, and W. Heink, "Principles and Applications of Self-Diffusion Measurements by Nuclear Magnetic Resonance," *Adv. Magn. Reson.*, **1988**, *12*, 1–89.
13. R. L. Haner and T. Schleich, "Measurement of Translational Motion by Pulse-Gradient Spin-Echo Nuclear Magnetic Resonance," *Methods Enzymol.*, **1989**, *176*, 418–446.
14. P. T. Callaghan and A. Coy, "PGSE NMR and Molecular Translational Motion in Porous Media," in *NMR Probes and Molecular Dynamics*, P. Tycko, Ed. Kluwer, Dordrecht, 1994, pp. 489–523.
15. D. Canet and M. Décorps, "Applications of Field Gradients in NMR," in *Dynamics of Solutions and Fluid Mixtures*, J.-J. Delpuech, Ed. Wiley, New York, 1995, pp. 309–343.
16. J. Kärger, "Diffusion in Porous Media," in *Encyclopedia of Nuclear Magnetic Resonance*, D. M. Grant and R. K. Harris, Eds. Wiley, New York, 1996, pp. 1656–1663.
17. C. S. Johnson, Jr., "Diffusion Measurements by Magnetic Field Gradient Methods," in *Encyclopedia of Nuclear Magnetic Resonance*, D. M. Grant and R. K. Harris, Eds. Wiley, New York, 1996, pp. 1626–1644.
18. K. J. Packer, "Diffusion & Flow in Liquids," in *Encyclopedia of Nuclear Magnetic Resonance*, D. M. Grant and R. K. Harris, Eds. Wiley, New York, 1996, pp. 1615–1626.
19. W. S. Price, "Gradient NMR," in *Annual Reports on NMR Spectroscopy*, G. A. Webb, Ed. Academic Press, London, 1996, pp. 51–142.
20. R. Mills and H. G. Hertz, "Application of the Velocity Cross-Correlation Method to Binary Nonelectrolyte Mixtures," *J. Phys. Chem.*, **1980**, *84*, 220–224.
21. W. S. Price, P. W. Kuchel, and B. A. Cornell, "Microviscosity of Human Erythrocytes Studied with Hypophosphite and ^{31}P-NMR," *Biophys. Chem.*, **1989**, *33*, 205–215.
22. W. S. Price and L.-P. Hwang, "Some Recent Developments in NMR Approaches for Studying Liquid Molecular Dynamics and their Biological Applications," *J. Chin. Chem. Soc. (Taipei)*, **1992**, *39*, 479–496.
23. W. S. Price, B. E. Chapman, and P. W. Kuchel, "Correlation of Viscosity and Conductance with ^{23}Na^{+}NMR T_1 Measurements," *Bull. Chem. Soc. Jpn.*, **1990**, *63*, 2961–2965.
24. J. McConnell, *Nuclear Magnetic Relaxation in Liquids*, Cambridge University Press, Cambridge, 1987.
25. P. Debye, *Polar Molecules*, Dover Publications, New York, 1945.
26. N. Bloembergen, E. M. Purcell, and R. V. Pound, "Relaxation Effects in Nuclear Magnetic Resonance Absorption," *Phys. Rev.*, **1948**, *73*, 679–712.
27. J. W. Hennel and J. Klinowski, *Fundamentals of Nuclear Magnetic Resonance*, Longman Scientific & Technical, Essex, 1993.
28. W. S. Price, B.-C. Perng, C.-L. Tsai, and L.-P. Hwang, "Microviscosity of Human Erythrocytes Studied using Hypophosphite Two-Spin Order Relaxation," *Biophys. J.*, **1992**, *61*, 621–630.
29. D. Canet, "Radiofrequency Gradient Pulses," in *Encyclopedia of Nuclear Magnetic Resonance*, D. M. Grant and R. K. Harris, Eds., Wiley, New York, 1996, pp. 3938–3944.
30. D. Canet, "Radiofrequency Field Gradient Experiments," *Progr. NMR Spectrosc.*, **1997**, *30*, 101–135.
31. R. E. Hurd, "Gradient-Enhanced Spectroscopy," *J. Magn. Reson.*, **1990**, *87*, 422–428.

32. P. C. M. Van Zijl and C. T. W. Moonen, "Complete Water Suppression for Solutions of Large Molecules Based on Diffusional Differences between Solute and Solvent (DRYCLEAN)," *J. Magn. Reson.*, **1990**, *87*, 18–25.
33. P. C. M. Van Zijl and C. T. W. Moonen, "Solvent Suppression Strategies for In Vivo Magnetic Resonance Spectroscopy," *NMR Basic Princ. Progr.*, **1992**, *26*, 67–108.
34. J. Keeler, R. T. Clowes, A. L. Davis, and E. D. Laue, "Pulsed-Field Gradients: Theory and Practice," *Methods Enzymol.*, **1994**, *239*, 145–207.
35. J. R. Tolman and J. H. Prestegard, "Homonuclear Correlation Experiments Using Pulsed-Field Gradients," *Concepts Magn. Reson.* **1995**, *7*, 247–262.
36. J.-M. Zhu and I. C. P. Smith, "Selection of Coherence Transfer Pathways by Pulsed-Field Gradients in NMR Spectroscopy," *Concepts Magn. Reson.* **1995**, **7**, 281–291.
37. R. E. Hurd, "Field Gradients & Their Application," in *Encyclopedia of Nuclear Magnetic Resonance*, D. M. Grant and R. K. Harris, Eds. Wiley, New York, 1996, pp. 1990–2005.
38. T. Parella, "High-Quality 1D Spectra by Implementing Pulsed-Field Gradients as the Coherence Pathway Selection Procedure," *Magn. Reson. Chem.*, **1996**, *34*, 329–347.
39. W. S. Price and Y. Arata, "The Manipulation of Water Relaxation and Water Suppression in Biological Systems Using the Water-PRESS Pulse Sequence," *J. Magn. Reson.*, **1996**, *B112*, 190–192.
40. W. S. Price, K. Hayamizu, and Y. Arata, "Optimization of the Water-PRESS Pulse Sequence and Its Integration into Pulse Sequences for Studying Biological Molecules," *J. Magn. Reson.*, in press.
41. P. T. Callaghan, *Principles of Nuclear Magnetic Resonance Microscopy*, Clarendon Press, Oxford, 1991.
42. S. L. Talagala and I. J. Lowe, "Introduction to Magnetic Resonance Imaging," *Concepts Magn. Reson.*, **1991**, *3*, 145–159.
43. Y. Xia, "Contrast in NMR Imaging and Microscopy," *Concepts Magn. Reson.*, **1996**, *8*, 205–225.
44. W. S. Price, "NMR Imaging," in *Annual Reports on NMR Spectroscopy*, G. A. Webb, Ed., Academic Press, London, 1997.
45. P. J. Basser, J. Mattiello, and D. Le Bihan, "MR Diffusion Tensor Spectroscopy and Imaging," *Biophys. J.*, **1994**, *66*, 259–267.
46. O. Henriksen, "Diffusion: Clinical Utility of MRI Studies," in *Encyclopedia of Nuclear Magnetic Resonance*, D. M. Grant and R. K. Harris, Eds. Wiley, New York, 1996, pp. 1605–1614.
47. D. Le Bihan, "Diffusion & Perfusion in MRI," in *Encyclopedia of Nuclear Magnetic Resonance*, D. M. Grant and R. K. Harris, Eds. Wiley, New York, 1996, pp. 1645–1656.
48. M. E. Moseley and A. de Crespigny, "Anisotropically Restricted Diffusion in MRI," in *Encyclopedia of Nuclear Magnetic Resonance*, D. M. Grant and R. K. Harris, Eds. Wiley, New York, 1996, pp. 834–839.
49. C. Pierpaoli, P. Jezzard, P. J. Besser, A. Barnett, and G. Di Chiro, "Diffusion Tensor MR Imaging of the Human Brain," *Radiology*, **1996**, *201*, 637–648.
50. C. Decanniere, S. Eleff, D. Davis, and P. C. M. Van Zijl, "Correlation of Rapid Changes in the Average Water Diffusion Constant and the Concentrations of Lactate and ATP Breakdown Products during Global Ischemia in Cat Brain," *Magn. Reson. Med.*, **1995**, *34*, 343–352.
51. G. Arfken, *Mathematical Methods for Physicists*, Academic Press, New York, 1995.
52. M. Abramowitz and I. A. Stegun, *Handbook of Mathematical Functions*, Dover, New York, 1970.
53. I. S. Gradshteyn and I. M. Ryzhik, *Table of Integrals, Series, and Products*, Academic Press, New York, 1994.
54. E. O. Stejskal and J. E. Tanner, "Spin Diffusion Measurements: Spin Echoes in the Presence of a Time-Dependent Field Gradient," *J. Chem. Phys.*, **1965**, *42*, 288–292.
55. E. O. Stejskal, "Use of Spin Echoes in a Pulsed Magnetic-Field Gradient to Study Anisotropic Restricted Diffusion and Flow," *J. Chem. Phys.*, **1965**, *43*, 3597–3603.
56. J. E. Tanner and E. O. Stejskal, "Restricted Self-Diffusion of Protons in Colloidal Systems by the Pulsed-Gradient, Spin-Echo Method," *J. Chem. Phys.*, **1968**, *49*, 1768–1777.
57. E. L. Hahn, "Spin Echoes," *Phys. Rev.*, **1950**, *80*, 580–594.
58. H. Y. Carr and E. M. Purcell, "Effects of Diffusion on Free Precession in Nuclear Magnetic Resonance Experiments," *Phys. Rev.*, **1954**, *94*, 630–638.
59. A. G. Avent, "Spin Echo Spectroscopy of Liquid Samples," in *Encyclopedia of Nuclear Magnetic Resonance*, D. M. Grant and R. K. Harris, Eds. Wiley, New York, 1996, pp. 4524–4530.
60. D. C. Douglass and D. W. McCall, "Diffusion in Paraffin Hydrocarbons," *J. Chem. Phys.*, **1958**, *62*, 1102–1107.
61. P. A. Egelstaff, *An Introduction to the Liquid State*, Oxford Science Publications, Oxford, 1994.
62. J. Crank, *The Mathematics of Diffusion*, Oxford University Press, Oxford, 1975.
63. J. Kärger and W. Heink, "The Propagator Representation of Molecular Transport in Microporous Crystallites," *J. Magn. Reson.*, **1983**, *51*, 1–7.
64. L. Debnath, *Integral Transforms and Their Applications*, CRC Press, Boca Raton, FL, 1995.
65. N. G. Van Kampen, *Stochastic Processes in Physics and Chemistry*, North Holland, Amsterdam, 1981.

66. H. S. Carslaw and J. C. Jaeger, *Conduction of Heat in Solids*, Oxford University Press, Oxford, 1959.
67. R. Lamanna, M. Delmelle, and S. Cannistraro, "Solvent Stokes-Einstein Violation in Aqueous Protein Solutions," *Phys. Rev.*, **1994**, *E49*, 5878–5880.
68. R. Mills, "Self-Diffusion in Normal and Heavy Water in the Range 1–45 Degrees," *J. Phys. Chem.*, **1973**, *77*, 685–688.
69. H. Weingärtner, "Self-Diffusion in Liquid Water. A Reassessment," *Z. Phys. Chem.*, **1982**, *132*, 129–149.
70. W. S. Price and P. W. Kuchel, "Restricted Diffusion of Bicarbonate and Hypophosphite Ions Modulated by Transport in Suspensions of Red Blood Cells," *J. Magn. Reson.*, **1990**, *90*, 100–110.
71. W. S. Price, B. E. Chapman, B. A. Cornell, and P. W. Kuchel, "Translational Diffusion of Glycine in Erythrocytes Measured at High Resolution with Pulsed Field Gradients," *J. Magn. Reson.*, **1989**, *83*, 160–166.
72. J. H. Wang, "Theory of Self-diffusion of Water in Protein Solutions. A New Method for Studying the Hydration and Shape of Protein Molecules," *J. Am. Chem. Soc.*, **1954**, *76*, 4755–4763.
73. P. T. Callaghan and J. Lelievre, "The Size and Shape of Amylopectin: A Study Using Pulsed Field Gradient Nuclear Magnetic Resonance," *Biopolymers*, **1985**, *24*, 441–460.
74. H. Jóhannesson and B. Halle, "Solvent Diffusion in Ordered Macrofluids: A Stochastic Simulation Study of the Obstruction Effect," *J. Chem. Phys.*, **1996**, *104*, 6807–6817.
75. H. C. Torrey, "Bloch Equations with Diffusion Terms," *Phys. Rev.*, **1956**, *104*, 563–565.
76. A. Abragam, *The Principles of Nuclear Magnetism*, Clarendon Press, Oxford, 1961.
77. Maple V. Release 4, Waterloo Maple, Inc., Waterloo, ON, Canada, 1996.
78. W. S. Price and P. W. Kuchel, "Effect of Nonrectangular Field Gradient Pulses in the Stejskal and Tanner (Diffusion) Pulse Sequence," *J. Magn. Reson.*, **1991**, *94*, 133–139.
79. C. H. Neuman, "Spin Echo of Spins Diffusing in a Bounded Medium," *J. Chem. Phys.*, **1974**, *60*, 4508–4511.
80. D. W. McCall, D. C. Douglass, and E. W. Anderson, "Self-Diffusion Studies by Means of Nuclear Magnetic Resonance Spin-Echo Techniques," *Ber. Bunsenges. Phys. Chem.*, **1963**, *67*, 336–340.
81. P. T. Callaghan, C. D. Eccles, and Y. Xia, "NMR Microscopy of Dynamic Displacement: ***k***-Space and ***q***-Space Imaging," *J. Phys.*, **1988**, *E21*, 820–822.
82. A. G. Marshall and F. R. Verdun, *Fourier Transforms in NMR, Optical, and Mass Spectroscopy: A User's Handbook*, Elsevier, Amsterdam, 1990.
83. P. A. Angelidis, "Spectrum Estimation and the Fourier Transform in Imaging and Spectroscopy," *Concepts Magn. Reson.*, **1996**, *8*, 339–381.
84. P. T. Callaghan, "Pulsed Field Gradient Nuclear Magnetic Resonance as Probe of Liquid State Molecular Organization," *Aust. J. Phys.*, **1984**, *37*, 359–387.
85. P. T. Callaghan, D. MacGowan, K. J. Packer, and F. O. Zelaya, "High-Resolution *q*-Space Imaging in Porous Structures," *J. Magn. Reson.*, **1990**, *90*, 177–182.
86. G. Fleischer and F. Fujara, "NMR as a Generalized Incoherent Scattering Experiment," *NMR Basic Princ. Progr.*, **1994**, *30*, 157–207.
87. P. T. Callaghan, "NMR Imaging, NMR Diffraction and Its Applications of Pulsed Gradient Spin Echoes in Porous Media," *Magn. Reson. Imaging*, **1996**, *14*, 701–709.
88. D. A. McQuarrie, *Statistical Mechanics*, Harper & Row, New York, 1976.
89. P. T. Callaghan, A. Coy, D. MacGowan, K. J. Packer, and F. O. Zelaya, "Diffraction-like Effects in NMR Diffusion of Fluids in Porous Solids," *Nature*, **1991**, *351*, 467–469.
90. D. G. Cory and A. N. Garroway, "Measurement of Translational Displacement Probabilities by NMR: An Indicator of Compartmentation," *Magn. Reson. Med.*, **1990**, *14*, 435–444.
91. P. T. Callaghan, A. Coy, D. MacGowan, and K. J. Packer, "Diffusion of Fluids in Porous Solids Probed by Pulsed Field Gradient Spin Echo NMR," *J. Mol. Liquids*, **1992**, *54*, 239–251.
92. M. Appel, G. Fleischer, D. Geschke, J. Kärger, and M. Winkler, "Pulsed-Field-Gradient NMR Analogue of the Single-Slit Diffraction Pattern," *J. Magn. Reson.*, **1996**, *A122*, 248–250.
93. P. Mansfield and P. K. Grannel, "'Diffraction' and Microscopy in Solids and Liquids by NMR," *Phys. Rev.*, **1975**, *B12*, 3618–3634.
94. P. Linse and O. Söderman, "The Validity of the Short-Gradient-Pulse Approximation in NMR Studies of Restricted Diffusion. Simulations of Molecules Diffusing between Planes, in Cylinders and Spheres," *J. Magn. Reson.*, **1995**, *A116*, 77–86.
95. K. J. Packer, "Oil Reservoir Rocks Examined by MRI," in *Encyclopedia of Nuclear Magnetic Resonance*, D. M. Grant and R. K. Harris, Eds. Wiley, New York, 1996, pp. 3365–3375.
96. P. P. Mitra and P. N. Sen, "Effects of Microgeometry and Surface Relaxation on NMR Pulsed-Field-Gradient Experiments: Simple Pore Geometries," *Phys. Rev.*, **1992**, *B45*, 143–156.
97. P. P. Mitra and P. N. Sen, "Effects of Surface Relaxation on NMR Pulsed Field Gradient Experiments in Porous Media," *Physica*, **1992**, *A186*, 109–114.
98. L. L. Latour, P. P. Mitra, R. L. Kleinberg, and C. H. Sotak, "Time-Dependent Diffusion Coefficient of Fluids in Porous Media as a Probe of Surface-to-Volume Ratio," *J. Magn. Reson.* **1993**, *A101*, 342–346.

99. A. Caprihan, L. Z. Wang, and E. Fukushima, "A Multiple-Narrow-Pulse Approximation for Restricted Diffusion in a Time-Varying Field Gradient," *J. Magn. Reson.*, **1996**, *A118*, 94–102.
100. D. Sheltraw and V. M. Kenkre, "The Memory-Function Technique for the Calculation of Pulsed-Gradient NMR Signals in Confined Geometries," *J. Magn. Reson.*, **1996**, *A122*, 126–136.
101. B. Balinov, B. Jönsson, P. L. Linse, and O. Söderman, "The NMR Self-Diffusion Method Applied to Restricted Diffusion. Simulation of Echo Attenuation from Molecules in Spheres and between Planes," *J. Magn. Reson.*, **1993**, *A104*, 17–25. Note: correction to Eq. [3] in *J. Magn. Reson.*, **1994**, *A108*, 130.
102. M. H. Blees, "The Effect of Finite Duration of Gradient Pulses on the Pulsed-Field-Gradient NMR Method of Studying Restricted Diffusion," *J. Magn. Reson.*, **1994**, *A109*, 203–209.
103. P. P. Mitra and B. I. Halperin, "Effects of Finite Gradient Pulse Widths in Pulsed Field Gradient Diffusion Measurements," *J. Magn. Reson.*, **1995**, *A113*, 94–101.
104. L. Z. Wang, A. Caprihan, and E. Fukushima, "The Narrow-Pulse Criterion for Pulsed-Gradient Spin-Echo Diffusion Measurements," *J. Magn. Reson.*, **1995**, *A117*, 209–219.
105. A. Coy and P. T. Callaghan, "Pulsed Gradient Spin Echo Nuclear Magnetic Resonance for Molecules Diffusing between Partially Reflecting Rectangular Barriers," *J. Chem. Phys.*, **1994**, *101*, 4599–4609.
106. J. S. Murday and R. M. Cotts, "Self-Diffusion Coefficient of Liquid Lithium," *J. Chem. Phys.*, **1968**, *48*, 4938–4945.
107. J. E. Tanner, "Transient Diffusion in a System Partitioned by Permeable Barriers. Application to NMR Measurements with a Pulsed Field Gradient," *J. Chem. Phys.*, **1978**, *69*, 1748–1754.
108. J. E. M. Snaar and H. Van As, "NMR Self-Diffusion Measurements in a Bound System with Loss of Magnetization at the Walls," *J. Magn. Reson.*, **1993**, *A102*, 318–326.
109. A. V. Barzykin, W. S. Price, K. Hayamizu, and M. Tachiya, "Pulsed Field Gradient NMR of Diffusive Transport through a Spherical Interface into an External Medium Containing a Relaxation Agent," *J. Magn. Reson.*, **1995**, *A114*, 39–46.
110. P. T. Callaghan, "Pulsed Gradient Spin Echo NMR for Planar, Cylindrical and Spherical Pores under Conditions of Wall Relaxation," J. Magn. Reson., **1995**, *A113*, 53–59.
111. P. W. Kuchel, A. J. Lennon, and C. J. Durrant, "Analytical Solutions and Simulations for Spin-Echo Measurements of Diffusion of Spins in a Sphere with Surface and Bulk Relaxation," *J. Magn. Reson.*, **1996**, B112, 1–17.
112. D. Le Bihan, "Molecular Diffusion, Tissue Microdynamics and Microstructure," *NMR Biomed.*, **1995**, *8*, 375–386.
113. E. W. Hsu, N. R. Aiken, and S. J. Blackband, "A Study of Diffusion Isotropy in Single Neurons by Using NMR Microscopy," *Magn. Reson. Med.*, **1997**, *37*, 624–627.
114. P. J. Basser, J. Mattiello, and D. Le Bihan, "Estimation of the Effective Self-Diffusion Tensor from the NMR Spin Echo," *J. Magn. Reson.*, **1994**, *B103*, 247–254.
115. B. L. Silver, *Irreducible Tensor Methods*, Academic Press, New York, 1976.
116. J. Mattiello, P. J. Basser, and D. Le Bihan, "Analytical Expressions for the *b* Matrix in NMR Diffusion Imaging and Spectroscopy," *J. Magn. Reson.*, **1994**, *A108*, 131–141.
117. O. Söderman and B. Jönsson, "Restricted Diffusion in Cylindrical Geometry," *J. Magn. Reson.*, **1995**, *A117*, 94–97.
118. S. R. de Groot and P. Mazur, *Non-Equilibrium Thermodynamics*, Dover, New York, 1984.
119. C. Pierpaoli and P. J. Basser, "Toward a Quantitative Assessment of Diffusion Anisotropy," *Magn. Reson. Med.*, **1996**, *36*, 893–906.
120. P. van Gelderen, D. Despres, P. C. M. Van Zijl, and C. T. W. Moonen, "Evaluation of Restricted Diffusion in Cylinders: Phosphocreatine in Rabbit Leg Muscle," *J. Magn. Reson.*, **1994**, *B103*, 255–260.
121. T. M. De Swiet and P. P. Mitra, "Possible Systematic Errors in Single-Shot Measurements of the Trace of the Diffusion Tensor," *J. Magn. Reson.*, **1996**, *B111*, 15–22.
122. G. Celebre, L. Coppola, and G. A. Raineri, "Water Self-Diffusion in Lyotropic Systems by Simulation of Pulsed Field Gradient Spin Echo Nuclear Magnetic Resonance Experiments," *J. Chem. Phys.*, **1992**, *97*, 7781–7785.
123. P. T. Callaghan, M. A. Le Gros, and D. N. Pinder, "The Measurement of Diffusion Using Deuterium Pulsed Gradient Nuclear Magnetic Resonance," *J. Chem. Phys.*, **1983**, *79*, 6372–6381.
124. G. Celebre, L. Coppola, G. A. Ranieri, and M. Terenzi, "Analysis of the PFG-SE NMR Experiments in Lyotropic Mesophases: The Hexagonal Case," *Mol. Cryst. Liquid Cryst.*, **1994**, *238*, 117–123.
125. P. T. Callaghan, K. W. Jolley, and J. Lelievre, "Diffusion of Water in the Endosperm Tissue of Wheat Grains as Studied by Pulsed Field Gradient Nuclear Magnetic Resonance," *Biophys. J.*, **1979**, *28*, 133–142.

William S. Price received his B.Sc. and Ph.D. (Biochemistry) degrees from the University of Sydney in 1986 and 1990, respectively. His Ph.D. studies were under the supervison of Professor Philip W. Kuchel and Dr. Bruce A. Cornell. He did postdoctoral study at the Institute of Atomic and Molecular Science in Taipei, Taiwan (1990–1993) with Professor Lian-Pin Hwang and at the National Institute of Material and Chemical Research in Tsukuba, Japan (1993–1995) with Dr. Kikuko Hayamizu. In 1995 he joined the research staff at the Water Research Institute in Tsukuba, Japan and presently holds the position of Chief Scientist. His interests focus on the use of NMR techniques such as Pulsed Field Gradient NMR, NMR microscopy, spin relaxation, and solid state ^{2}H NMR to study molecular dynamics in chemical and biochemical systems.